ELSEVIER

Chemical Engineering Journal 114 (2005) 9–31

Chemical Engineering Journal

www.elsevier.com/locate/cej

An algorithm for predicting the hydrodynamic and mass transfer parameters in agitated reactors

Romain Lemoine, Badie I. Morsi *

Chemical and Petroleum Engineering Department, University of Pittsburgh, Pittsburgh, PA 15261 USA

Received 24 February 2005; received in revised form 10 August 2005; accepted 26 August 2005

Abstract

A large number of experimental data points (7374) obtained in our laboratory as well as from the literature, covering wide ranges of reactor geometry (reactor diameter and type, impeller diameter and gas distribution scheme), physicochemical properties (liquid and gas density and molecular weight, liquid viscosity and surface tension, diffusivity) and operating variables (superficial gas velocity, temperature, pressure, mixing speed, liquid height and mixtures) were used to develop empirical as well as back-propagation neural network (BPNN) correlations in order to predict the hydrodynamic and mass transfer parameters in gas–liquid agitated reactors (ARs). The empirical and BPNN correlations developed were incorporated in a calculation algorithm for predicting the gas holdup (ε_G), volumetric mass transfer coefficients (k_La), Sauter mean bubble diameter (d_S), gas–liquid interfacial area (a) and liquid-side mass transfer coefficient (k_L) in ARs, operating in surface-aeration, gas-inducing and gas-sparging modes.

The algorithm was used to predict the effects of liquid viscosity and hydrogen mole fraction in the feed gas ($H_2 + N_2$) on the hydrodynamic and mass transfer parameters for the soybean oil hydrogenation process conducted in a large-scale gas-sparging agitated reactor (7000 kg soybean oil capacity). The predictions showed that increasing the liquid-phase viscosity, mimicking the evolution of the hydrogenation of soybean oil in a batch reactor, decreased ε_G and increased d_S, resulting in a decrease of a. The decrease of the gas holdup with increasing the liquid-phase viscosity was related to the increase of gas bubble coalescence in the reactor. Increasing liquid-phase viscosity, however, decreased k_L as well as k_La values for both H_2 and N_2 within the range H_2 mole fraction (0–1) used. This k_L behavior indicated that the effect of viscosity on k_L is more significant than that of d_S, since k_L was reported to be proportional to d_S. The predictions also showed that increasing the H_2 mole fraction in the feed to the reactor decreased ε_G and increased d_S, resulting in a decrease of a and an increase of k_L as well as k_La for both H_2 and N_2 within the range of liquid-phase viscosity used (0.0023–0.0047 Pa s). The decrease of the gas holdup with increasing the H_2 mole fraction in the feed gas was attributed to the decrease of the density (momentum) of the gas mixture. The increase of k_L values with increasing the H_2 mole fraction in the feed gas was related to the increase of d_S. The predicted k_La values indicated that the mass transfer behavior in the large-scale gas-sparging reactor proposed for soybean oil hydrogenation was controlled by the mass transfer coefficient, k_L. Also, under similar conditions, k_La values for H_2 in soybean oil when using the gaseous mixture ($H_2 + N_2$) were lower than those obtained for H_2 (as a single-component); and k_L values for H_2 were consistently greater than those of N_2 within the ranges of the operating conditions used in the simulation.

Keywords: Hydrodynamics; Mass transfer; Agitated reactors; Scale-up

1. Introduction

Agitated reactors (ARs) are suitable for slow-reaction regime processes, such as most liquid-phase oxidation, hydrogenation, chlorination and some fermentation processes. This is because ARs are characterized by high liquid holdup and mass/heat transfer, which are required to maintain the gas concentration in the liquid bulk close to saturation, insuring high performances [1]. The use of one or several impellers for agitation purposes increases the contact time between the gas and the liquid phases via circulation and intensifies the heat transfer between the phases and the cooling coils or reactor walls, leading to effective temperature control which is essential for achieving optimal performance of most gas–liquid processes. ARs can be employed in series or in cascade of agitated reactors for large throughput commercial gas–liquid processes [2,3]. Also, the flexible mode of operation of ARs as depicted in Fig. 1 (gas-sparging, gas-inducing and surface-aeration)

* Corresponding author. Tel.: +1 4126249650; fax: +1 4126249639.
E-mail address: morsi@engrng.pitt.edu (B.I. Morsi).

1385-8947/$ – see front matter © 2005 Elsevier B.V. All rights reserved.
doi:10.1016/j.cej.2005.08.015

Nomenclature

a	gas–liquid interfacial area per unit liquid of the gas bubbles, m^{-1}
a_{Wave}	gas–liquid interfacial area per unit liquid of gas–liquid surface, m^{-1}
d_S	Sauter mean bubble diameter, m
D_{AB}	diffusivity of gas in the liquid, $m^2\,s^{-1}$
$d_{Imp.}$	diameter of the impeller, m
d_T	diameter of the tank, m
g	gravitational constant, $m\,s^{-2}$
H	liquid height, m
H_L	liquid height above the last impeller, m
k_L	liquid-side mass transfer coefficient, $m\,s^{-1}$
k_La	volumetric liquid-side mass transfer coefficient, s^{-1}
M_W	molecular weight, $kg\,kmol^{-1}$
N	mixing speed, Hz
N_{CR}	critical mixing speed, Hz
N_{CRE}	critical mixing speed of gas entrainment, Hz
N_{CRI}	critical mixing speed of gas induction, Hz
$n_{Imp.}$	number of impeller
P	pressure, bar
P^*/V_L	total (mechanical + gas) power input per unit volume, $W\,m^{-3}$
Q_{GI}	induced gas flow rate, $m^3\,s^{-1}$
R	gas constant, $MPa\,m^3\,kmol^{-1}\,K^{-1}$
T	temperature, K
U_G	superficial gas velocity, $m\,s^{-1}$
$u_{0,i}$	bias of first hidden layer
$u_{i,j}$	weight of first hidden layer
U_T	terminal gas velocity, $m\,s^{-1}$
$v_{0,i}$	bias of second hidden layer
$v_{i,j}$	weight of second hidden layer
V_L	volume of the liquid, m^3
w_0	bias of output layer
w_i	weight of output layer
X_W	concentration of the major component in a liquid mixture, wt
y_{H_2}	mole fraction of hydrogen in the gas mixture

Greek symbols

ε_G	gas holdup
μ_L	viscosity, $kg\,m^{-1}\,s^{-1}$
ρ_G	density of the gas, $kg\,m^{-3}$
ρ_L	density of the liquid, $kg\,m^{-3}$
σ_L	surface tension of the liquid, $N\,m^{-1}$
σ	standard of deviation $= \sqrt{\frac{1}{n-1}\sum_1^n\left(\left\|\frac{Z_{Pred.}-Z_{Exp.}}{Z_{Exp.}}\right\| - AARE\right)^2} \times 100\%$

Dimensionless numbers

Aeration number: $Ae = \frac{Q_G}{N \times d_{Imp.}^3}$

Aeration number modified: $Ae^* = \frac{U_G}{N \times d_{Imp.}}$

Critical Froude number: $Fr_C = \frac{d_{Imp.}^2 \times N_{CR}^2}{g \times H_L}$

Euler number: $Eu = \frac{P_T}{d_{Imp.}^2 \times \rho_L \times N^2}$

Froude number: $Fr = \frac{d_{Imp.}^2 \times N^2}{g \times H_L}$

Froude number modified: $Fr^* = \frac{d_{Imp.} \times N^2}{g}$

Re-circulation number: $N_{cir} = d_{Imp.} N \times \left(\frac{\rho_L}{g\sigma_L(\rho_L - \rho_G)}\right)^{1/4}$

Power number $N_P = \frac{P^*}{\rho_L N^3 d_{Imp.}^5}$

Reynolds number: $Re = \frac{d_{Imp.}^2 \times \rho_L \times N}{\mu_L}$

Schmidt number: $Sc = \frac{\mu_L}{\rho_L \times D_A}$

Sherwood number: $Sh = \frac{k_L a \times d_{Imp.}^2}{D_A}$

Weber number: $We = \frac{d_{Imp.}^3 \times \rho_L \times N^2}{\sigma_L}$

Acronyms

AARE	average absolute relative error $= \frac{1}{n}\sum_1^n \left\|\frac{Z_{Pred.}-Z_{Exp.}}{Z_{Exp.}}\right\| \times 100\%$
ANN	artificial neural network
BPNN	back-propagation neural network
DT	draft tube
GIR	gas-inducing reactor
GSR	gas-sparging reactor
HS	hollow shaft
I.V.	iodine value
SAR	surface-aeration reactor

Subscripts

G	gas
L	liquid
T	total
W	water
*	reduced

makes them suitable for reactions requiring extremely safe conditions.

In gas-sparging reactors (GSRs), the gas is bubbled through the liquid at a given superficial velocity from a distributor located at the bottom of the reactor underneath the impeller, which is used for mixing the gas and liquid phases. In gas-inducing reactors (GIRs), holes are machined on the hollow shaft of the reactor and are located in the gas and liquid phases. Due to the angular velocity of the impeller, a pressure drop between the top and bottom of the shaft is created, which induces the gas into the liquid-phase. In surface-aeration reactors (SARs), the impeller provides the mixing and the gas absorption into the liquid-phase takes place mainly through the gas–liquid interface. Thus, the hydrodynamic and mass transfer parameters are expected to be different for these three operating modes. The SARs have the simplest design, however, the rate of gas absorption in such reactors is expected to be the lowest when compared with those in

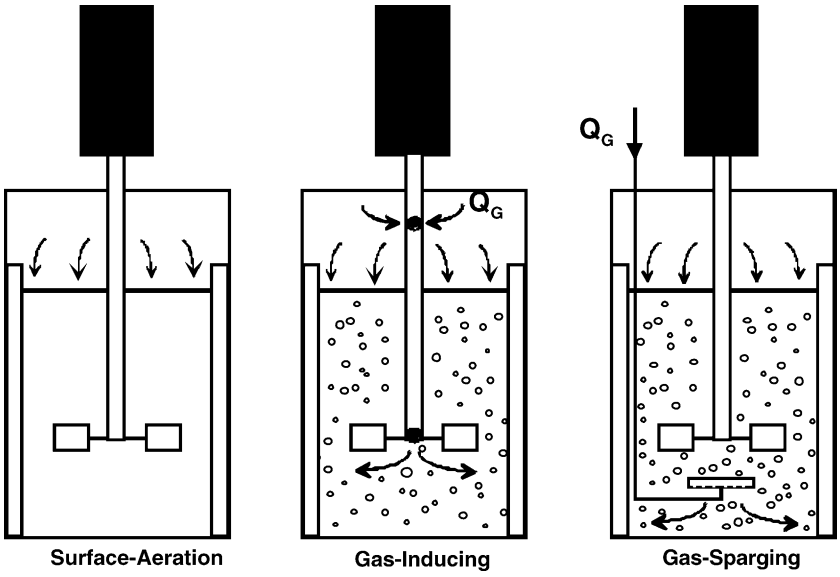

Fig. 1. Operation modes of agitated reactors.

GIRs and GSRs. The GIRs have higher rate of gas absorption and gas holdup than those in the SARs without any additional costs or the need for re-circulation loop. The GSRs enjoy the highest gas absorption rate and gas holdup, however, the need for a compressor to sparge the gas into these reactors could be costly.

The design, scale-up and optimal operations of ARs require, among others, the knowledge of the hydrodynamics, mass trans-

Table 1
Literature correlations of d_S in ARs

Authors	Gas/liquid	Reactors	Operating conditions	Correlations
Vermeulen et al. [6]	–	GSR	Atm.	$d_S = 0.00429 \times \frac{\sigma_L \mu_L^{0.25}}{N^{1.5} d_{Imp.} \rho_L^{0.50} \mu_G^{0.75}} \times e^{[1.072+0.626\times\ln(\varepsilon_G)+0.0733\times(\ln(\varepsilon_G))^2]}$
Calderbank [7]	Air/H_2O, C_7H_8, alcohols, glycols, CCl_4, nitro-benzene, ethyl acetate	GSR	Atm. N: 3.3–20 Hz; U_G: 3–6 × 10^{-3} m s^{-1}; d_T: 0.18, 0.51 m	$d_S = 4.15 \times \frac{\sigma_L^{0.6}}{(P^*/V_L)^{0.4} \rho_C^{0.2}} \times \varepsilon_G^{1/2} + 0.0009$
Miller [8]	CO_2, air/aqueous solution	GSR	Atm. N: 0.4–7 Hz; U_G: 8–150 × 10^{-3} m s^{-1}; d_T: 0.15–0.67 m	$d_S = 4.15 \times \sigma_L^{0.6} \left(\frac{P_G^*}{V_L}\right)^{0.4} \rho_L^{0.2} \times \varepsilon_G^{1/2} + 0.0009$
Shridhar and Potter [9]	Air/cyclohexane	GSR	T: 298–423 K; P: 0.1–1 MPa; N: 8–30 Hz; U_G: <0.032 m s^{-1}; d_T: 0.13 m	$d_S = 4.15 \times \frac{\sigma_L^{0.6}}{(P_G^*/V_L)^{0.4} \rho_C^{0.2}} \left(\frac{\rho_{AIR}}{\rho_G}\right)^{0.16} \left(\frac{P_G^*}{E_T}\right) \varepsilon_G^{1/2} + 0.0009$
Hughmark [10]	–	GSR	–	$\frac{d_S g \rho_L}{\sigma_L} = 5.5 \times \varepsilon_G^{1/2} \left(\frac{N^2 d_{Imp.}^3}{d_{Imp.} g V_L^{2/3}} (P_G^*/P^*)^{2/3}\right)^{1/2}$
Matsumura et al. [11]	O_2/water + sodium alginate	SAR	Atm. N: 7–16.5 Hz; d_T: 0.218 m	$d_S = 7.67 \times 10^{-2} \times \left(\frac{\mu_L^2}{g\rho_L^2}\right)^{1/3} \left(\frac{N_2 d_{Imp.} \mu_L}{\sigma_L}\right)^{-0.10} \times \left(\frac{N_2^3 d_{Imp.}^3 \rho_L}{\mu_L g}\right)^{0.50} \left(\frac{U_E}{N_2 d_{Imp.}}\right)^{0.22}$ [a]
Parthasarathy et al. [12]	Air/water + methyl isobutyl carbinol	GSR	Atm. N: 2–13.3 Hz; U_G: 0.2–1 × 10^{-3} m s^{-1}; d_T: 0.065 m	$d_S = 2.0 \times \sigma_L^{3/5} \left(\frac{P_G^*}{V_L}\right)^{-2/5} \rho_L^{-1/5}$
Fillion [13]	H_2, N_2/soybean oil	GIR; GSR	P: 0.1–0.5 MPa; T: 373–473 K; N: 10–23.3 Hz; Q_G: 0.01–0.05 m^3 s^{-1}; d_T: 0.11 m	$d_{S\text{-GIR}} = 3.00 \times \frac{\sigma_L^{0.60} Q_G^{0.38}}{(P_G^*/V_L)^{0.04} \rho_L^{0.20}}$, $d_{S\text{-GSR}} = 0.436 \times M_W^{-0.01} \frac{\sigma_L^{0.60} Q_G^{0.20}}{(P_G^*/V_L)^{0.06} \rho_L^{0.20}}$

[a] N_2 is the lower impeller mixing speed.

Table 2
Literature correlations of the gas holdup in ARs

Authors	Gas/liquid	Reactors	Operating conditions	Correlations
Calderbank [7]	Air/H_2O, C_7H_8, alcohols, glycols, CCl_4, nitro-benzene, ethyl acetate	GSR	Atm. N: 3.3–20 Hz; U_G: 3–6 × 10^{-3} m s^{-1}; d_T: 0.18, 0.51 m	$\varepsilon_G = \left(\frac{U_G \varepsilon_G}{U_T}\right)^{1/2} + 0.000216 \times \left(\frac{P^*}{V_L}\right)^{0.4} \rho_C^{0.2}/\sigma_L^{0.6} \times \left(\frac{U_G}{U_T}\right)^{1/2}$
Rushton and Bimbinet [14]	Air/H_2O + corn syrup	GSR	Atm. U_G: 3–30 × 10^{-3} m s^{-1}; d_T: 0.23–0.91 m	$\varepsilon_G = a \times \left(\frac{P_G^*}{V_L}\right)^b U_G^c$ a and b constants function of $d_{Imp.}/d_T$, $c = 0.6$
Miller [8]	CO_2, air/aqueous solution	GSR	Atm. N: 0.4–7Hz; U_G: 8–150 × 10^{-3} m s^{-1}; d_T: 0.15–0.67 m	$\varepsilon_G = \left(\frac{U_G \varepsilon_G}{U_T + U_G}\right)^{1/2} + 0.000216 \times \left(\frac{P_G^*}{V_L}\right)^{0.4} \rho_C^{0.2}/\sigma_L^{0.6} \times \left(\frac{U_G}{U_T + U_G}\right)^{1/2}$
Loiseau et al. [15]	Air/water, glycol, water + alcohols, sodium sulfite	GSR	Atm. N: 5–50 Hz; U_G: 0.7–85 × 10^{-3} m s^{-1}; d_T: 0.22 m	$\varepsilon_G = 0.011 \times U_G^{0.360} \sigma_L^{-0.360} \mu_L^{-0.056} \times \left(\frac{P^*}{V_L} + \frac{\rho_G Q_G RT}{M_G V_L \ln(P_{Sparger}/P_T)}\right)^{0.270}$
Matsumura et al. [16]	Water, alcohols	GSR	Atm. N: 7–16.5 Hz; U_G: 0.5–10 × 10^{-3} m s^{-1}; d_T: 0.218 m	$\varepsilon_G = 6.86 \times 10^{-3} Re^{0.180} We^{0.250} \times Ae^{*-0.200} Fr^{*0.335}$
Lopes de Figueiredo and Calderbank [17]	O_2/water	GSR	Atm. N: 5–8 Hz; P^*/V_L: 0.41–4.8 kW m^{-3}; d_T: 0.91 m	$\varepsilon_G = 0.34 \times \left(\frac{P_G^*}{V_L}\right)^{1/4} U_G^{3/4}$
Shridhar and Potter [9]	Air/cyclohexane	GSR	P: 0.1–1 MPa; T: 298–423 K; N: 8–30 Hz; U_G: <0.032 m s^{-1}; d_T: 0.13 m	$\varepsilon_G = \left(\frac{\varepsilon_G U_G}{U_T}\right)^{1/2} + 0.000216 \times \left(\frac{P_G^*}{V_L}\right)^{0.4} \rho_C^{0.2}/\sigma_L^{0.6} \times \left(\frac{U_S}{U_T}\right)^{1/2} \left(\frac{\rho_G}{\rho_{AIR}}\right)^{0.16} \left(\frac{E_T}{P_G^*}\right)$
Hughmark [10]	–	GSR	–	$\varepsilon_G = 0.74 \times \left(\frac{Q_G}{NV_L}\right)^{0.5} \left(\frac{N^2 d_{Imp.}^4}{d_{Imp.} g V_L^{0.67}}\right)^{0.5} \times \left(\frac{N^2 d_{Imp.}^4 d_S}{\sigma_L V_L^{0.67}}\right)^{0.25}$
Matsumura et al. [11]	O_2/water + sodium alginate	SAR	Atm. N: 7–16.5 Hz; d_T: 0.218 m	$\varepsilon_G = 2.16 \times \left(\frac{N_2 d_{Imp.} \mu_L}{\sigma_L}\right)^{0.30} \left(\frac{N_2^3 d_{Imp.}^3 \rho_L}{\mu_L g}\right)^{0.30} \times \left(\frac{U_E}{N_2 d_{Imp.}}\right)^{1.05}$ [a]
He et al. [18]	Air/water + CMC, water + Triton-X-114	GIR	Atm. N: 3.3–33.3 Hz; d_T: 0.075 m	$\varepsilon_G = 3.19 \times 10^{-4} \left(\frac{P_G^*}{V_L}\right)^{1.90}$ $\varepsilon_G = 5.85 \times 10^{-3} \left(\frac{P_G^*}{V_L}\right)^{0.95}$ [b,c]
Al Taweel and Cheng [19]	Air/water + PGME	GIR	Atm. N: 12.5–25 Hz; d_T: 0.19 m	$\varepsilon_G = 10^{14.5} N^{1.77} Q_G^{0.25} \sigma_L^{-10.4}$ for air/water + additives
Heim et al. [20]	Air/water-fermentation mixture	GIR	Atm. Fr^*: 0.28–1.49; Re: 33–260 × 10^3; d_T: 0.3 m	$\varepsilon_G = 28.96 \times Fr^{0.968} Re^{-0.354} Ae^{0.644} \times \left(\frac{d_{Imp.}}{H_L}\right)^{0.176}$ [d] $\varepsilon_G = 199.70 \times Fr^{1.063} Re^{-0.458} Ae^{0.789} \times \left(\frac{d_{Imp.}}{H_L}\right)^{0.316}$ [e] $\varepsilon_G = 25.85 \times Fr^{0.947} Re^{-0.336} Ae^{0.634} \times \left(\frac{d_{Imp.}}{H_L}\right)^{0.255}$ [f]
Wichterle [21]	H_2O, glycerin, CCl_4, tenside, ethylioside	SAR	Atm. d_T: 0.57–0.9 m	$\varepsilon_G = 0.12 \times (N_{cir} - 1.4 \times N_{cir_E})$ for $N_{cir} > 1.4 N_{cir_E}$, otherwise $\varepsilon_G = 0$

Table 2 (*Continued*)

Authors	Gas/liquid	Reactors	Operating conditions	Correlations
Saravanan and Joshi [22]	Air/H_2O	GIR	Atm. N: 0.3–15.5 Hz; d_T: 0.57,1,1.5 m	$\varepsilon_G = 2.67 \times 10^{-3}\left(\frac{d_{Imp.}}{d_T}\right)^{1.63}\left(\frac{N^2 Q_G \rho_L}{\mu_L g}\right)^{0.48}$
Tekie [3]	N_2, O_2/cyclohexane	GIR	P: 0.7–3.5 MPa; T: 330–430 K; N: 6.7–20 Hz; d_T: 0.11 m	$\varepsilon_G = 3.85 \times 10^{-2} \times \left(\frac{N-N_0}{N_0}\right)^{1.19}\left(\frac{\mu_G}{\mu_L}\right)^{-0.74} \times \left(\frac{\rho_G}{\rho_L}\right)^{0.82}\left(\frac{\sigma_L}{\sigma_{L0}}\right)^{1.97}$ with $\sigma_{L0} = 0.025\ \mathrm{N\,m^{-1}}$, $N_0 = 11.6$ Hz
Murugesan [23]	Air/water, toluene, glycerol	GSR	Atm. N: 3.3–23.3 Hz; U_G: 1–66 $\times 10^{-3}$ m s^{-1}; d_T: 0.15 m	$\varepsilon_G = 31.2 \times U_G^{0.5}\left(\frac{\rho_L^2}{\sigma_L \Delta\rho_L g}\right)^{0.125}\left(\frac{N^2 d_T}{g}\right)^{0.45} \times \left(\frac{\mu_L^4 g}{\sigma^3 \rho}\right)^{0.08}\left(\frac{d_W}{d_T}\right)^{0.85}\left(\frac{d_{Imp.}}{d_T}\right)^{0.65}$
Fillion [13]	H_2, N_2/soybean oil	GIR	P: 0.1–0.5 MPa; T: 373–473 K; N: 10–23.3 Hz; d_T: 0.11 m	$\varepsilon_G = 1.151 \times M_W^{0.07}(Fr - Fr_C)^{0.41} Ae^{0.52}$

[a] N_2 is the lower impeller mixing speed.
[b] $(P_G^*/V_L) < 20\ \mathrm{kW\,m^{-3}}$.
[c] $(P_G^*/V_L) > 20\ \mathrm{kW\,m^{-3}}$.
[d] For a 4-pipe impeller.
[e] For a 6-pipe impeller.
[f] For a disk impeller.

fer/heat transfer, and reaction kinetics under actual process conditions in large-scale reactors. Literature data indicate that the gas–liquid mass transfer is generally the rate-limiting step in many industrial processes [4], and therefore the focus of this study is on the determination of the hydrodynamic and mass transfer parameters in ARs. Several studies have been devoted to the determination of the hydrodynamics and mass transfer parameters in ARs [5–44]. Unfortunately, the majority of these studies have been carried out under ambient conditions using aqueous systems, with the exception of few studies conducted under high pressures and temperatures as detailed in Tables 1–3.

In general, available literature correlations for predicting the hydrodynamic and mass transfer are based on dimensionless numbers, specific mixing power input, non-linear statistical approach or artificial neural networks (ANNs) as can be observed in Tables 1–3. The dimensionless numbers and specific mixing power input correlations, supposedly independent of the gas–liquid system, often provide large deviations when compared with experimental data [45–47]. The statistical correlations are specific to the gas–liquid system and reactor employed, even though they enjoy high confidence levels [43]. Also, artificial neural networks have been successfully employed to correlate the volumetric mass transfer coefficients (k_La) in GSRs [45,46] and in SARs as well as GIRs [47]; however, to our knowledge no work could be found in the literature on the use of ANNs for predicting the hydrodynamic parameters in these three types of ARs.

Thus, there is a great need to develop correlations for predicting the hydrodynamics and mass transfer parameters in agitated reactors, which would be system-independent and could further be used for proper design and scale-up of industrial processes. Therefore, the goal of this study is to use a large number of experimental data points (7374) obtained in our laboratory and from the literature, covering wide ranges of operating conditions, agitated reactor geometries and sizes, to develop empirical and ANNs correlations, which will be incorporated into an algorithm for predicting systematically the hydrodynamic and mass transfer parameters in ARs. The developed algorithm is then used to predict the effect of operating variables on the hydrodynamic and mass transfer parameters in the soybean oil hydrogenation process.

2. Correlations of the hydrodynamic and mass transfer parameters

Predicting the hydrodynamic and mass transfer parameters in ARs is a difficult task, since these parameters can be affected, among others, by: (1) geometrical variables: reactor diameter (d_T), impeller diameter ($d_{Imp.}$) and impeller height from the bottom of the reactor (H_F); (2) operating variables: reactor mode (SAR, GIR and GSR), mixing speed (N), liquid height (H), liquid height above the impeller (H_L), temperature (T) and gas partial pressure (P) and (3) physicochemical variables: liquid viscosity (μ_L), liquid and gas densities (ρ_L and ρ_G), liquid surface tension (σ_L), gas diffusivity in the liquid (D_{AB}) and impurities/mixture composition (X_W). In order to develop generalized correlations for predicting the hydrodynamic and mass transfer parameters in ARs, a large database (7374 data points) obtained in our laboratories and from the literature as shown in Table 4, were first used to develop empirical correlations and then ANN correlations, which are more powerful and can easily manipulate non-linear input–output relationships than empirical correlations.

Table 3
Literature correlations of k_La in ARs

References	Gas/liquid	Reactor	Operating conditions	Correlation
Robinson and Wilke [26]	N_2, CO_2/aqueous solutions	GSR	Atm. 303 K; N: 6.7–36.7 Hz; U_G: 1–4.6 10^{-3} m s^{-1}; P^*/V_L: 0.03–18 kW m^{-3}; d_T: 0.15 m	$k_La = 3.89 \times 10^{-3} \times \left(\frac{P^*_G}{V_L}\right)^{0.74} U_G^{0.36}$
Perez and Sandall [27]	CO_2/carbopol solution	GSR	Atm. T: 297–308 K; N: 3–8 Hz; U_G: 0.162–0.466 m s^{-1}; d_T: 0.15 m	$\frac{d^2_{Imp.}k_La}{D_{AB}} = 21.2 \times \left(\frac{N\rho_L d^2_{Imp.}}{\mu_{eff}}\right)^{1.11} \left(\frac{\mu_{eff}}{\rho_L D_{AB}}\right)^{0.5} \times \left(\frac{d_{Imp.}U_G}{\sigma_L}\right)^{0.447} \left(\frac{\mu_G}{\mu_{eff}}\right)^{0.694}$ [a]
Bern et al. [28]	H_2/fat	GSR	P: 0.12–0.14 MPa; T: 453 K; N: 3–12.5 Hz	$k_La = c \times \left(\frac{N^{3.15}d_T^{5.35}}{V_L^{1.41}}\right)^n U_G^m$ [b]
Matsumura et al. [24]	O_2, air/H_2O, various alcohols	SAR	Atm. N: 7–16.5 Hz; d_T: 0.218 m	$\frac{k_La}{\sqrt{D_{AB}}} = 309 \times \left(\frac{P^*}{V_L}\right)^{0.6} \varepsilon_G^{0.6}$
Joshi and Sharma [29]	CO_2/Na_2CO_3 + $NaHCO_3$	GIR	Atm. N: 3–11.7 Hz; U_G: 0.0003–0.032 m s^{-1}; P^*/V_L: 1–15 kW m^{-3}; d_T: 0.41–1.0 m	For $U_G < 0.005$: $k_La = 6.8 \times 10^{-3}\left(\frac{P^*}{V_L}\right)^{0.55} U_G^{0.5}$ For $U_G > 0.005$: $k_La = 3.26 \times 10^{-3}\left(\frac{P^*}{V_L}\right)^{0.55} U_G^{0.25}$
Lopes de Figueiredo and Calderbank [17]	O_2/water	GSR	Atm. N: 5–8 Hz; P_G:0.41–4.8 kW m^{-3}; U_G: 6–13 × 10^{-3} m s^{-1}; d_T: 0.91 m	$\frac{k_La V_L}{d_T} = 10^{-3} \times (P^*)^{0.58} U_G^{0.75}$
Matsumura et al. [30]	O_2, CO_2, CH_4/sodium sulfite, H_2O	GSR	Atm. N: 7–16.5 Hz; U_G: 0.5–10 × 10^{-3}m s^{-1}; d_T: 0.218 m	$\frac{k_La}{\sqrt{D_{AB}}} = 3.09 \times 10^2 \times \left(\frac{P^*_G}{V_L}\right)^{0.6} \varepsilon_G^{0.6}$
Kara [31]	H_2/tetralin SRCII	GIR	P: 7–13.5 MPa; T: 606–684 K; N: 0.8–6.6 Hz; d_T: 0.076 m	$k_La = (3.42 \pm 1.13) \times 10^{-4}\left(\frac{P^*}{V_L}\right)^{0.80\pm0.009}\left(\frac{H_L}{D_T}\right)^{-1.9\pm0.66}$
Sawant et al. [32]	Air/water + sodium sulfate	GIR	Atm. N: 5–36 Hz; d_T: 0.1 × 0.1–0.38 × 0.38 m	$k_La = 0.0195 \times \left(\frac{P^*}{V_L}\right)^{0.5}$
Judat [33]		GSR	–	$k_La = 9.8 \times 10^{-5}(B^{-0.6} + 0.81 \times 10^{-0.65/B})^{-1} \times \left(\frac{P^*}{V_L\rho_L(\mu_L g^4)^{1/3}}\right)^{0.4}\left(\frac{\mu_L}{\rho_L g^2}\right)^{-1/3}$ [c]
Albal et al. [25]	O_2/H_2O, CMC	SAR	Atm. N: 1.7–16.76 Hz; d_T: 0.1 m	$Sh = 1.41 \times 10^{-2} Sc^{0.5} Re^{0.67} We^{1.29}$
Karandikar et al. [34]	CO, H_2, CO_2, CH_4/F-T wax + water	GIR	P: 0.7–4.5 MPa; T: 423–498 K; N: 11.6–16.6 Hz; d_T: 0.13 m	$k_La_{CO,H_2} = 0.1607 \times (N/1000)^{3.42} \exp \times (0.108 \times P) - 0.046$ $k_La_{CO_2,CH_4} = 0.0171 \times (N/1000)^{6.05} \exp \times (0.38 \times P) + 0.00525$
Versteeg et al. [35]	CO_2, N_2O/H_2O, aq. alkanol-amine	SAR	P: 0.1–1.0 MPa; T: 291–356 K; Re: 0.2–1.2 × 10^4; Sc: 0.1–1.3 × 10^4	$Sh = 0.064 \times Sc^{0.5} Re^{0.72}$
Chang [36]	H_2,CO_2,CH_4/n-C_6, n-C_{10}, n-C_{14}	GIR	Eu: 0.5–1 × 10^4; Sc: 8–500; Re: 0.3–3 × 10^5, Fr^*: 1–3; We: 1–7 × 10^4	$Sh_{H_2} = 2.74 \times 10^{-18} Re^{3.00} Sc^{2.21} Eu^{-0.42} We^{1.29}$ $Sh_{CO,CH_4} = 5.114 \times 10^{-12} Re^{2.18} Sc^{1.63} Eu^{0.28} Fr^{*1.73}$
Hichri et al. [37]	H_2/2-propanol, o-cresol	GIR	Sh: 0.1–5 × 10^5; V_G/V_L: 1–2; Re: 0.7–13 × 10^4; Sc: 5–9 × 10^3; We: 2–6 × 10^3	$Sh = 0.123 \times Re^{0.44} Sc^{0.5} We^{1.27}\left(\frac{V_G}{V_L}\right)^{1.1}$
Dietrich et al. [38]	H_2/H_2O, ethanol, hydrogenation mixture	GIR	Atm. N: 14–33 Hz; d_T: 0.07 m	For $H/D_T = 1$: $Sh = 3 \times 10^{-4} Re^{1.45} Sc^{0.5} We^{0.5}$ For $H/D_T = 1.4$: $Sh = 1.5 \times 10^{-4} Re^{1.45} Sc^{0.5} We^{0.5}$
Koneripalli et al. [39]	H_2, CO, CO_2/methanol, ethanol	GIR	Eu: 0.3–10 × 10^3; We: 0.2–2 × 10^4; Sc: 7–200, Re: 0.6–4 × 10^5	$Sh = 4.88 \times 10^6 Re^{-3.81} Sc^{0.23} We^{4.48} Eu^{0.09}$

Table 3 (*Continued*)

References	Gas/liquid	Reactor	Operating conditions	Correlation
Mizan et al. [40]	H_2, C_2H_4/C_3H_6	SAR	Fr^*: 0.9–2.0; Re: 2–4.5 × 10^5; We: 741–31060	$Sh = 55.2 \times Fr^{*2.07} Re^{1.20} We^{-1.34}$
Heim et al. [20]	Air/water-fermentation mixture	GIR	Atm. Fr: 0.28–1.49; Re: 33–260 × 10^3; d_T: 0.3 m	$\frac{Sh^*}{9.5 \times 10^{-5}} = 1 - e^{-19.64 Re^{-0.216} Fr^{1.336}}$ d,e,f $\frac{Sh^*}{1.06 \times 10^{-4}} = 1 - e^{-21.63 Re^{-0.234} Fr^{1.207}}$ $\frac{Sh^*}{1.04 \times 10^{-4}} = 1 - e^{-1331.20 Re^{-0.557} Fr^{2.498}}$
Wu [41]	Air/H_2O + Na_2SO_3 + $CoSO_4$	SAR	Atm. P^*/V_L: 1.2–8.5 kW m^{-3}	$k_La = 6.34 \times 10^{-2} \left(\frac{P^*}{V_L}\right)^{0.65}$
Yoshida et al. [42]	Air/water	GSR	Atm. N: 2.5–6.7 Hz; U_G: 0.004–0.06 m s^{-1}	$k_La = 2.5 N^{1.5(1.7\times10^{-7})^{U_G}\,1.06^{n_{Imp.}}} U_G^{1.29} n_{Imp.}^{0.10}$
Tekie [3]	N_2, O_2/cyclohexane	SAR; GIR	SAR; x_1: 6.67–20.0 Hz; x_2: 0.7–3.5 MPa; x_3: 330–430 K; x_4: 0.171–0.268 m; GIR; x_1: 6.67–20.0 Hz; x_2: 0.7–3.5 MPa; x_3: 330–430 K; x_4: 0.171–0.268 m	$Sh_{SAR} = 4.51 \times 10^3 We^{-0.21} Fr^{0.92}$ $\ln(k_La_{SAR\text{-}N_2}) = -2.90 + 0.36x_1 + 0.07x_2 + 0.28x_3 - 0.18x_4 - 0.39x_1^2 - 0.06x_2^2 + 0.04x_3^2 + 0.063x_4^2 - 2.90e^{(-0.2(x_1-0.204)^2)} + 0.04e^{(0.1(x_1+3)(4-x_4))}$ $\ln(k_La_{SAR\text{-}O_2}) = -2.93 + 0.11x_1 + 0.10x_2 + 0.23x_3 - 0.12x_4 - 0.38x_1^2 - 0.05x_2^2 - 0.03x_3^2 + 0.07x_4^2 - 2.90e^{(-0.173(x_1)^2)} + 0.11e^{(0.1(x_1+3)(4-x_4))}$ $\ln(k_La_{GIR\text{-}N_2}) = 0.01 - 1.92x_1 + 0.10x_2 + 0.27x_3 - 0.05x_4 + 0.72x_1^2 - 0.10x_2^2 + 0.02x_3^2 + 0.01x_4^2 - 3.40e^{0.04(x_1-4.25)^2} + 0.27e^{0.1(x_1+3)(4-x_4)}$ $\ln(k_La_{GIR\text{-}O_2}) = -3.71 + 1.23x_1 + 0.11x_2 + 0.22x_3 - 0.09x_4 + 0.09x_1^2 - 0.04x_2^2 + 0.01x_3^2 + 0.06x_4^2 - 3.75e^{-0.17(x_1-1.6)^2} + 0.21e^{0.1(x_1+3)(4-x_4)}$
Tekie et al. [43]	N_2, O_2/cyclohexane	GIR	We: 0.2–1 × 10^4, Fr^*: 1–3	$Sh_{GIR} = 4.51 \times 10^3 We^{-0.21} Fr^{*0.92} \times (1 + 1.867 \times 10^3_{\varepsilon_G})$
Fillion [13]	N_2, H_2/soybean oil	GIR; GSR; SAR	GIR; x_1: 373–473 K; x_2: 10–23.3 Hz; x_3: 0.171–0.268 m; x_4: 0.1–0.5 MPa GSR; T: 373–473 K; N: 10–23.3 Hz; P: 0.1–0.5 MPa; U_G: 10.4–51.9 cm^3 s^{-1}; SAR; x_1: 373–473 K; x_2: 10–23.3 Hz; x_3: 0.171–0.268 m; x_4: 0.1–0.5 MPa	$\ln(k_La_{GIR\text{-}N_2}) = -4.86 - 0.18x_1 + 0.71x_2 - 0.60x_3 + 0.08x_1^2 + 0.12x_2^2 - 0.23x_1x_2 - 0.08x_2x_3 - 0.34x_1x_2x_3 - 0.07x_1^3 + 0.0027 \times (x_2 + 2.5)e^{2x_3} + 1.28\tan h(0.3x_2(5.5 - x_3^2) + 0.1(2 - 4x_3))$ $\ln(k_La_{GIR\text{-}H_2}) = -3.87 + 0.52x_2 - 0.79x_3 + 0.22x_1^2 - 0.35e^{x_1} + 0.33e^{x_3} - 0.0038(x_2 + 3)e^{2.5x_3} - 0.93x_1e^{-\lvert x_2\rvert} + 2.10\tan h(0.3x_2(8 - x_3^2) + 0.1(2 - 6x_3))$ $k_La_{GSR} = 1226 \times T\mu_L^{-0.10} D_{AB}^{0.62} \left(\frac{P_G^*}{V_L}\right)^{0.31} Q_G^{0.58}$ $\ln(k_La_{SAR\text{-}N_2}) = -6.50 + 0.177x_1 + 0.474x_2 - 0.407x_3 + 0.053x_3^2 - 0.0798x_2x_3$ $\ln(k_La_{SAR\text{-}H_2}) = -5.99 + 0.229x_1 + 0.417x_2 - 0.473x_3 - 0.0445x_1^2 + 0.0524x_3^2 - 0.126x_2x_3$

[a] $\mu_{eff} = \frac{\tau(\gamma_a)}{\gamma_a}$.
[b] $c = 0.326$, $n = 0.37 \pm 0.02$, $m = 0.32 \pm 0.10$, d_T (cm), U_S (cm s^{-1}), V_L (cm^3).
[c] $B = \frac{Q}{d_T^2} \times \left(\frac{\rho_L}{\mu_L g}\right)^{1/3}$.
[d] 4-pipe impeller.
[e] 6-pipe impeller.
[f] Disk impeller.

2.1. Empirical correlations

Previously, Lemoine et al. [73] proposed the following correlations for predicting the critical mixing speed for gas entrainment in the SAR (N_{CRE}), the critical mixing speed for gas induction in the GIR (N_{CRI}), the induced gas flow rate in the GIR (Q_{GI}) and the wavy gas–liquid interfacial area in the SAR (a_{Wave}):

Table 4
Database on ARs used in this study

References	Parameters	Gas/liquid	Reactor	Operating conditions	Legend
Rushton and Bimbinet [14]	ε_G	Air/ water + corn syrup	GSR	Atm. U_G: 3–30 × 10^{-3} m s^{-1}; d_T: 0.23–0.91 m	
Fuchs et al. [48]	N_{CRE}, k_La	Air, N_2, O_2/water	SAR; GSR	Atm. U_G: 0–53 × 10^{-3} m s^{-1}; d_T: 0.13–3.33 m	
Martin [49]	N_{CRI}, Q_{GI}	Air/water	GIR (HS)	Atm. N: 4.3–6.0 Hz; d_T: 0.280 m	
Miller [8]	ε_G, d_S, k_La	CO_2, air/aqueous solution	GSR	Atm. N: 0.4–7 Hz; U_G: 8–150 × 10^{-3} m s^{-1}; d_T: 0.15–0.67 m	
Robinson and Wilke [26]	ε_G, d_S, k_La	N_2, O_2, CO_2/water, alkaline solution	GSR	Atm. 303 K; N: 6.7–36.7 Hz; U_G: 1–4.6 × 10^{-3} m s^{-1}; d_T: 0.1524m	
Bern et al. [28]	k_La	H_2/fat	GSR	P: 0.12–0.14 MPa; T: 453 K; N: 3–12.5 Hz; U_G: 35–300 × 10^{-3} m s^{-1}; d_T: 0.25, 0.65, 2.4 m	
Loiseau [50]	ε_G, d_S, k_La	Air, O_2/water, glycol, ethanol, sugar, acetic acid, CuCl, sodium sulfite	GSR	Atm. N: 6.7–50.0 Hz; U_G: 0.75–85.0 × 10^{-3} m s^{-1}; d_T: 0.225 m	
Joshi and Sharma [29]	N_{CRI}, Q_{GI}, ε_G, d_S (a), k_La	CO_2, air/water, sodium dithionite, Na_2CO_3 + $NaHCO_3$	GIR (HS)	Atm. N: 3–11.7 Hz; d_T: 0.41, 0.57, 1.0 m	
Lopes de Figueiredo and Calderbank [17]	ε_G, d_S, k_La	O_2/water	GSR	Atm. N: 5–8 Hz; U_G: 6–13 × 10^{-3} m s^{-1}; d_T: 0.91 m	
Botton et al. [51]	N_{CRE}, ε_G, k_La	Air /water, glycol, sodium sulphite	SAR; GSR	Atm. N: 0–50 Hz; U_G: <0.1 m s^{-1}; d_T: 0.085, 0.12, 0.25, 0.60	
Shridhar and Potter [9]	ε_G, d_S	Air/cyclohexane	GSR	P: 0.1–1.0 MPa; N: 8–30 Hz; U_G: <0.032 m s^{-1}; d_T: 0.13 m	
Matsumura et al. [11]	N_{CRE}, d_S	Air, O_2/water + sodium alginate	SAR	Atm. N: 7–16.5 Hz; d_T: 0.190, 0.242, 0.316 m	
Greaves and Barigou [52]	ε_G	Air/water	GSR	Atm. N: 0.6–8.33 Hz; U_G: 6.3–10.7 × 10^{-3} m s^{-1}; d_T: 1.0 m	
Chang [36]	k_La	H_2, N_2, CO, CH_4/water, *n*-hexane, *n*-decane, *n*-tetradecane, cyclohexane	GIR (HS)	P: 0.5–5.96 MPa; T: 328–378 K; N: 13.3–20.0 Hz; d_T: 0.127 m	
He et al. [18]	N_{CRI}, ε_G	Air/water + CMC, water + Triton-X-114	GIR (HS)	Atm. N: 3.3–33.3 Hz; d_T: 0.075 m	
Smith et al. [53]	ε_G	Air/water	GSR	Atm. N: 0.45–4.0 Hz; U_G: 8.8–28.7 × 10^{-3} m s^{-1}; d_T: 1.2, 1.6, 1.8, 2.7 m	
Koneripalli [54]	k_La	N_2, CO, H_2, CH_4, CO_2/methanol, ethanol	GIR (HS)	P: 0.33–5.48 MPa; T: 328–428 K; N: 13.3–23.3 Hz; d_T: 0.127 m	
Mizan [55]	k_La	H_2, C_2H_4, C_3H_6/*n*-hexane, propylene	SAR	P: 0.16–3.16 MPa; T: 297–353 K; N: 13.3–20.0 Hz; d_T: 0.125 m	
Rielly et al. [56]	N_{CRI}, Q_{GI}	Air/water	GIR (HS)	Atm. N: 3.4–9.0 Hz; d_T: 0.3–0.6 m	
Rewatkar et al. [57]	ε_G	Air/water	GSR	Atm. N: 0.85–8.0 Hz; U_G: 6.3–30.0 × 10^{-3} m s^{-1}; d_T: 1.0, 1.5 m	
Aldrich and van Deventer [58]	N_{CRI}, Q_{GI}	Air/water, ethyl alcohol, sucrose solution	GIR (DT)	Atm. N: 9.2–20.0 Hz; d_T: 0.19 m	
Nienow et al. [59]	ε_G	Air/water, dirty water	GSR	Atm. N: 0.67–2.5 Hz; U_G: 10–75 × 10^{-3} m s^{-1}; d_T: 1.98 m	
Saravanan et al. [60]	N_{CRI}, Q_{GI}	Air/water	GIR (DT)	Atm. N: 0.13–13.5 Hz; d_T: 0.57, 1, 1.5 m	
Aldrich and van Deventer [61]	Q_{GI}	Air/water, brine, alcohol, sucrose solution	GIR (DT)	Atm. T: 291–350 K; N: 13.3–16.3 Hz; d_T: 0.19 m	
Al Taweel and Cheng [19]	ε_G	Air/water + PGME	GIR (DT)	Atm. N: 12.5–25 Hz; d_T: 0.19 m	
Li [62]	k_La	H_2, C_3H_8, C_2H_4, C_3H_6/propane, *n*-hexane	SAR	P: 0.14–5.8 MPa; T: 297–353 K; N: 13.3–20.0 Hz; d_T: 0.125 m	

Table 4 (*Continued*)

References	Parameters	Gas/liquid	Reactor	Operating conditions	Legend
Saravanan and Joshi [63]	N_{CRI}, Q_{GI}	Air /water	GIR (DT)	Atm. N: 0.3–15.45 Hz; d_T: 0.57, 1, 1.5 m	
Saravanan and Joshi [22]	ε_G	Air/H_2O	GIR (DT)	Atm. N: 0.3–15.5 Hz; d_T: 0.57, 1, 1.5 m	
Yoshida et al. [42]	ε_G, k_La	Air/water	GSR	Atm. N: 2.5–6.7 Hz; U_G: 4–60 × 10^{-3} m s^{-1}; d_T: 0.25 m	
Tekie [3]	d_S, k_La	N_2, O_2/cyclohexane	SAR; GIR (HS)	P: 0.7–3.5 MPa; T: 330–430 K; N: 6.7–20 Hz; d_T: 0.11	
Forrester et al. [64]	Q_{GI}, d_S, k_La	Air /water	GIR (HS)	Atm. N: 5.0–10.0 Hz; d_T: 0.45 m	
Murugesan [23]	ε_G	Air/water, toluene, glycerol	GSR	Atm. N: 3.3–23.3 Hz; U_G: 1–66 × 10^{-3} m s^{-1}; d_T: 0.15 m	
Solomakha and Tarasova [65]	ε_G, k_La	–	GSR	Atm. U_G: 2–87 × 10^{-3} m s^{-1}; d_T: 0.2–3.6 m	
Mohammad [66]	k_La	O_2, N_2/benzoic acid	SAR; GIR (HS)	P: 0.09–0.5 MPa; T: 473 K; N: 16.7 Hz; d_T: 0.076	
Patil and Joshi [67]	N_{CRI}, Q_{GI}	Air /water	GIR (DT)	Atm. N: 3.5–10.0 Hz; d_T: 1.0 m	
Vrabel et al. [68]	ε_G	Air /water, NaCl	GSR	Atm. N: 1.5–2.5 Hz; U_G: 10–40 × 10^{-3} m s^{-1}; d_T: 1.876, 2.09 m	
Bouaifi et al. [69]	ε_G, d_S, k_La	Air /water	GSR	Atm. N: 1.66–11.67 Hz; U_G: 0.54–2.63 × 10^{-3} m s^{-1}; d_T: 0.43 m	
Fillion [13]	N_{CRI}, Q_{GI}, ε_G, d_S, k_La	N_2, H_2/soybean oil	SAR; GIR (HS); GSR	P: 0.1–0.5 MPa; T: 373–473 K; N: 10–23.3 Hz; H: 0.171–0.268 m; Q_G: 10.4–51.9 × 10^{-6} m^3 s^{-1}; d_T: 0.115 m	
Poncin et al. [70]	N_{CRI}, Q_{GI}, ε_G, k_La	Air /water	SAR; GIR (HS)	Atm. d_T: 0.6 m	
Yawalkar et al. [71]	ε_G	Air /water	GSR	Atm. N: 1.0–11.0 Hz; U_G: 3.9–15.7 × 10^{-3} m s^{-1}; d_T: 0.57 m	
Alves et al. [72]	ε_G, d_S, k_La	Air O_2/water, sodium sulphate, PEG	GSR	Atm. N: 4.2–10.0 Hz; U_G: 2.5–5.0 × 10^{-3} m s^{-1}; d_T: 0.292 m	
Lemoine et al. [73]	N_{CRE}, N_{CRI}, Q_{GI}	Air, N_2/toluene, benzaldehyde, benzoic acid	SAR; GIR (HS)	P: 0.1–1.5 MPa; T: 300–453 K; N: 10.3–12.3 Hz; d_T: 0.125 m	
Linek et al. [74]	ε_G, k_La	Air, O_2/water, water + $NaSO_4$	GSR	Atm. N: 4.17–14.17 Hz; U_G: 2.12–8.48 × 10^{-3} m s^{-1}; d_T: 0.29 m	
Heintz [75]	N_{CRI}, Q_{GI}, ε_G, d_S, k_La	N_2, CO_2/fluorinated liquids	GIR(HS)	P: 0.2–3.0 MPa; T: 300–500 K; N: 10–12.3 Hz; d_T: 0.115 m	
Lemoine and Morsi [5]	ε_G, d_S, k_La	Air, N_2/toluene, benzaldehyde, benzoic acid	SAR; GIR (HS); GSR	P: 0.1–1.5 MPa; T: 300–453 K; N: 10.3–12.3 Hz; U_G: 0–4 × 10^{-3} m s^{-1}; d_T: 0.125 m	
Soriano [76]	k_La	CO, N_2, H_2, He/PAO-8, Sasol wax	GIR (HS)	P: 0.7–3.5 MPa; T: 423–523 K; N: 13.3–20.0 Hz; d_T: 0.076 m	

$$\frac{N_{CRE}^2 d_{Imp.}}{g} = 0.441 \times \left(\frac{\mu_L}{\mu_{Water}}\right)^{0.100} \left(\frac{\sigma_L}{\sigma_{Water}}\right)^{-0.430} \times \left(\frac{\rho_L}{\rho_{Water}}\right)^{2.960} \left(\frac{H_L}{d_T}\right)^{-0.100} e^{0.378 H_L/d_{Imp.}} \quad (1)$$

$$\frac{N_{CRI}^2 d_{Imp.}}{g} = 0.512 \times \left(\frac{\mu_L}{\mu_{Water}}\right)^{0.146} \left(\frac{\sigma_L}{\sigma_{Water}}\right)^{-0.180} \times \left(\frac{\rho_L}{\rho_{Water}}\right)^{-0.265} \left(\frac{H_L}{d_T}\right) \quad (2)$$

$$Ae = \frac{Q_{GI}}{N d_{Imp.}^3} = 50.03 \times \frac{n_{Imp.}^{1.695} d_T^{2.584} \mu_L^{0.627} \rho_L^{1.991} \rho_G^{2.847}}{\sigma_L^{4.440} M_{W_{Gas}}^{3.203}} \times \exp\left(-3.957 \times \frac{Eu^{0.142} We^{0.174}}{Re^{0.048} (Fr - Fr_C)^{0.042}}\right) \quad (3)$$

$$a_{Wave} = \frac{1}{H} + \frac{1}{H_L} \times \frac{Re^{1.75} We^{3.00}}{Eu^{3.00}} \left(\frac{\rho_L}{\rho_G}\right)^{-2.67} \times e^{-12.95 \times H - 0.59 \times N} \quad (4)$$

In this study, 7374 experimental points obtained in our laboratories as well as from the literature on hydrodynamic and

Table 5
Upper and lower limits of the variables used in Eqs. (1)–(29)

Variables	Maximum value	Minimum value
U_G, m s^{-1}	0.3	0
N, Hz	54.0	0
H, m	6.542	0.064
H_L, m	4.97	1.15×10^{-2}
d_T, m	3.600	0.075
$d_{Imp.}$, m	1.370	0.032
ρ_L, kg m^{-3}	2042	310
μ_L, Pa s	0.09	5.00×10^{-5}
σ_L, N m^{-1}	0.077	1.20×10^{-3}
ρ_G, kg m^{-3}	194.90	0.05
X_W, wt.	1.0000	0.5589
D_{AB}, 10^9 m^2 s^{-1}	153.94	0.08
$n_{Imp.}$	8	1
$M_{W\text{-}Gas}$, kg kmol^{-1}	44	2

mass transfer parameters were used to develop empirical correlations for predicting the gas holdup (ε_G), the Sauter mean bubble diameter (d_S) and the volumetric mass transfer coefficient (k_La) in SARs, GIRs and GSRs. Table 5 lists the ranges of operating variables, physical properties and reactor geometry used in these correlations.

For predicting the gas holdup in the SARs:

$$\varepsilon_{G\text{-}SAR} = 16.3 \times \left(\frac{P^*_{SAR}}{V_L}\right)^{\alpha_{SAR}} (Fr - Fr_C)^{\beta_{SAR}} \quad (5)$$

$$\alpha_{SAR} = -0.573 \times d_T^{-0.142} N^{-0.400} \mu_L^{-0.137} \rho_G^{0.101} \quad (6)$$

$$\beta_{SAR} = 1.36 \times 10^{-5} \times d_{Imp.}^{0.001} H_L^{-0.001} N^{0.130} \rho_L^{1.920} \mu_L^{0.932} \times \sigma_L^{-1.360} \quad (7)$$

For predicting the gas holdup in the GIRs:

$$\varepsilon_{GIR} = 0.102 \times \left(\frac{P^*_{GIR}}{V_L}\right)^{\alpha_{GIR}} U_G^{\beta_{GIR}} \times \exp(-0.349 X_W) \quad (8)$$

$$\alpha_{GIR} = 3.770 \times 10^{-5} \times d_T^{-2.540} N^{0.005} \mu_L^{-0.012} \sigma_L^{-0.603} \rho_G^{-0.122} \quad (9)$$

$$\beta_{GIR} = 0.087 \times d_{Imp.}^{-0.819} H_L^{0.617} N^{-0.854} \rho_L^{-0.036} \mu_L^{-0.043} \sigma_L^{-0.560} \quad (10)$$

For predicting the gas holdup in the GSRs:

$$\varepsilon_{G\text{-}GSR} = 9.620 \times 10^{-3} \times \left(\frac{P^*_{GSR}}{V_L}\right)^{\alpha_{GSR}} U_G^{\beta_{GSR}} \times \exp(-0.216 X_W) \quad (11)$$

$$\alpha_{GSR} = 0.190 \times d_T^{-0.179} N^{0.043} \mu_L^{-0.228} \sigma_L^{0.261} \rho_G^{-0.011} \quad (12)$$

$$\beta_{GSR} = 1.86 \times 10^{12} \times d_{Imp.}^{-0.087} H_L^{-0.279} N^{0.063} \rho_L^{-4.270} \mu_L^{-0.464} \times \sigma_L^{1.380} \quad (13)$$

It should be mentioned that the quantity (P^*/V_L) is the total energy dissipated which corresponds to the sum of the power input (impeller and gas sparged) per unit liquid volume [44]. Several correlations to predict the impeller and gas power input per unit liquid volume for SARs [16,21], GIRs [20,29,60,70] and GSRs [8–10,15,44,50,69] can be found in the Appendix. It is also important to point out that in GIRs and GSRs, X_W was introduced in Eqs. (8) and (11) in order to account for the liquid composition and its foamability [77]. Even though the foamability or froth formation in liquid mixtures is a complex phenomenon, the choice of this variable was found to fit fairly well literature experimental findings, and therefore it was used in this study. X_W represents the concentration of the primary liquid in the mixture, and its value lies between 0.50 and 1. Consequently, for a single-component and for a complex organic liquid mixture composed of more than three hydrocarbons, such as oils and waxes, X_W equals 1.

For predicting the Sauter mean bubble diameter in SARs:

$$d_{S\text{-}SAR} = 1.31 \times 10^{-3} \times (Fr - Fr_C)^{\gamma_{SAR}} \varepsilon_{G\text{–}SAR}^{\lambda_{SAR}} \quad (14)$$

$$\gamma_{SAR} = -5.81 \times 10^{-6} \times d_{Imp.}^{-1.310} d_T^{1.550} N^{1.300} \mu_L^{-0.588} \quad (15)$$

$$\lambda_{SAR} = 0.207 \times \rho_L^{-0.408} \sigma_L^{-0.171} \rho_G^{-0.141} H_L^{-0.657} \quad (16)$$

For predicting the Sauter mean bubble diameter in GIRs:

$$d_{S\text{-}GIR} = 2.61 \times 10^{-3} \times U_G^{\gamma_{GIR}} \varepsilon_{G\text{–}GIR}^{\lambda_{GIR}} \quad (17)$$

$$\gamma_{GIR} = 3.980 \times 10^{-2} \times d_{Imp.}^{1.500} d_T^{-2.020} N^{0.419} \mu_L^{0.102} \quad (18)$$

$$\lambda_{GIR} = 3.310 \times 10^{-2} \times \rho_L^{0.373} \sigma_L^{-0.044} \rho_G^{-0.093} H_L^{0.070} \times \exp(-1.180 X_W) \quad (19)$$

For predicting the Sauter mean bubble diameter in GSRs:

$$d_{S\text{-}GSR} = 9.380 \times 10^{-3} \times U_G^{\gamma_{GSR}} \varepsilon_{G\text{–}GSR}^{\lambda_{GSR}} \quad (20)$$

$$\gamma_{GSR} = 1.380 \times 10^{-2} \times d_{Imp.}^{-0.878} d_T^{0.351} N^{0.563} H_L^{0.185} \quad (21)$$

$$\lambda_{GSR} = 1.300 \times 10^{-20} \times \rho_L^{7.490} \sigma_L^{-0.240} \rho_G^{-0.196} \times \exp(-8.470 X_W) \quad (22)$$

Also, for predicting the volumetric mass transfer coefficient in SARs:

$$k_L a_{SAR} = 69.961 \times \frac{D_{AB}^{0.500}}{\rho_G^{0.060}} \left(\frac{P^*_{SAR}}{V_L}\right)^{\delta_{SAR}} \times \left(2.678 \times 10^{-2} + \frac{(2.085 \times 10^{-3} + d_S)^{0.155} \varepsilon_G^{0.234}}{(Fr - Fr_C)^{-\eta_{SAR}}}\right) \quad (23)$$

$$\delta_{SAR} = 0.925 \times d_{Imp.}^{1.156} N^{0.348} H_L^{-0.830} \quad (24)$$

$$\eta_{SAR} = 0.010 \times d_T^{-2.820} N^{3.570} \mu_L^{-0.679} \sigma_L^{3.998} \quad (25)$$

For predicting the volumetric mass transfer coefficient in GIRs:

$$k_L a_{GIR} = 1.383 \times 10^5 \times \frac{D_{AB}^{0.500} \varepsilon_G^{0.155} d_S^{0.414}}{\rho_G^{0.060}} \left(\frac{P^*_{GIR}}{V_L} \right)^{\delta_{GIR}} \times U_G^{\eta_{GIR}} \exp(-2.011 X_W) \quad (26)$$

$$\delta_{GIR} = 7.010 \times 10^{-6} \times d_{Imp.}^{-0.395} d_T^{4.183} N^{2.237} \mu_L^{0.126} H_L^{-0.658} \quad (27)$$

$$\eta_{GIR} = 0.420 \times d_{Imp.}^{-2.385} d_T^{-2.485} N^{-3.238} \sigma_L^{-0.261} H_L^{3.249} \quad (28)$$

For predicting the volumetric mass transfer coefficient in GSRs:

$$k_L a_{GSR} = 2.564 \times 10^3 \times \frac{D_{AB}^{0.500} \varepsilon_G^{0.575}}{\rho_G^{0.060} d_S^{0.402}} \left(\frac{P^*_{GSR}}{V_L} \right)^{\delta_{GSR}} \times U_G^{\eta_{GSR}} \exp(-2.402 X_W) \quad (29)$$

$$\delta_{GSR} = 4.664 \times 10^{-4} \times d_T^{0.124} N^{0.593} \mu_L^{-0.769} \quad (30)$$

$$\eta_{GSR} = 9.475 \times 10^{-5} \times d_{Imp.}^{0.363} N^{0.967} \rho_L^{-0.470} \mu_L^{-0.884} H_L^{-1.440} \quad (31)$$

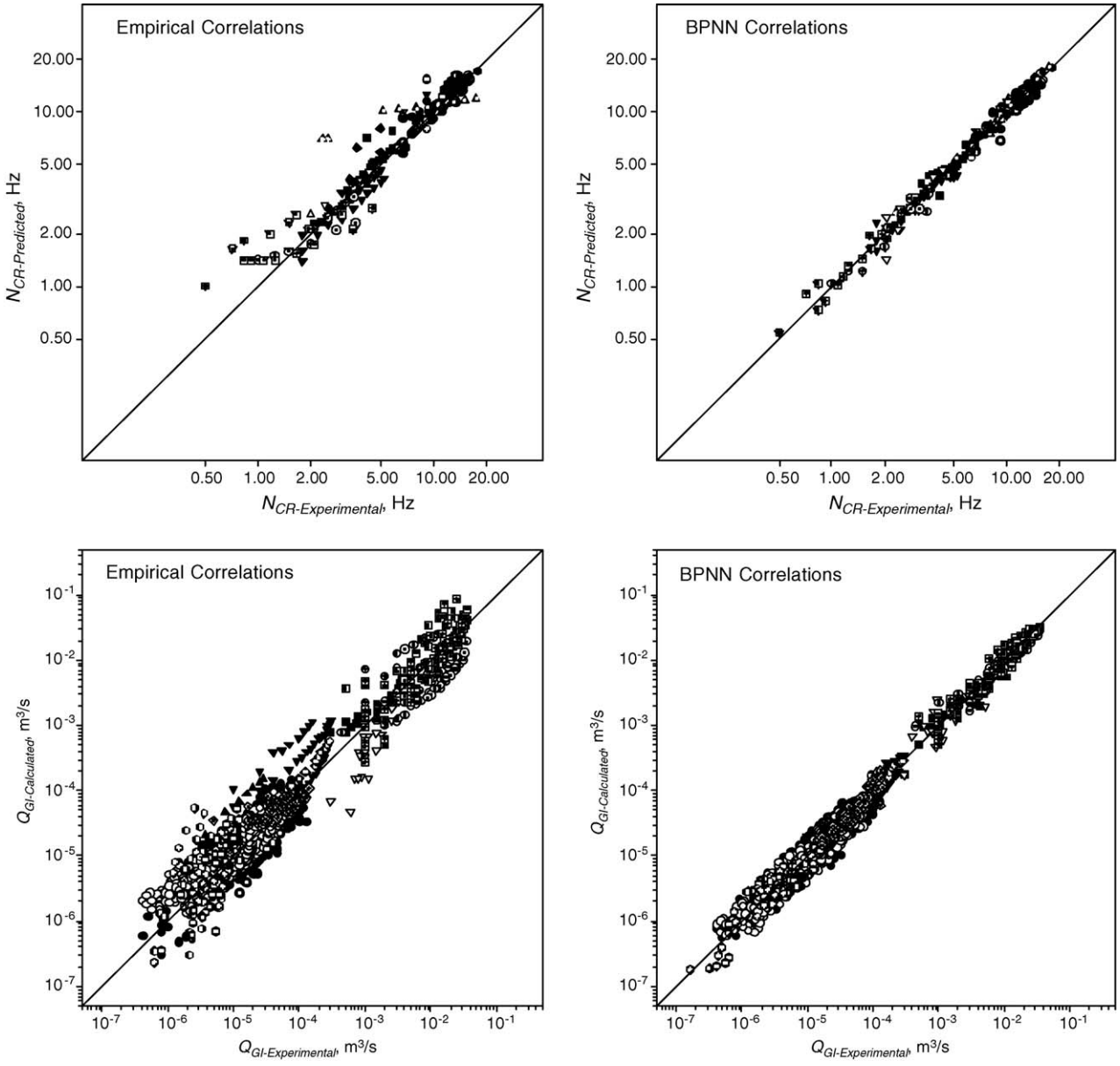

Fig. 2. Comparison between experimental and predicted N_{CR} and Q_{GI} values using empirical and BPNN correlations.

Table 6
Architecture and input variables of the N_{CR}, Q_{GI}, ε_G, d_S, a_{Wave} and k_La BPNN correlations

Parameters	$\ln N_{CR}$			$\ln Q_{GI}$			$\ln \varepsilon_G$			$\ln d_S$			$\ln k_La$			$\ln a_{Wave}H$		
	Max 7.762		Min 3.401	Max −3.324		Min −15.613	Max −0.528		Min −9.871	Max −4.720		Min −8.557	Max −0.265		Min −8.093	Max 0.452		Min 0
Variables	Position in BPNN	Max	Min	Position in BPNN	Max	Min	Position in BPNN	Max	Min	Position in BPNN	Max	Min	Position in BPNN	Max	Min	Position in BPNN	Max	Min
Reactor type	1	1	0	–	–	–	1	1	0	1	1	0	–	–	–	–	–	–
H, m	2	6.227	0.064	1	1.67	0.14	3	6.542	0.082	–	–	–	–	–	–	–	–	–
H_L, m	3	4.66	1.15×10^{-2}	2	1.000	0.083	12	4.97	3.75×10^{-2}	–	–	–	–	–	–	–	–	–
U_G, m s^{-1}	–	–	–	–	–	–	4	0.3	0.0	3	0.3	0	2	0.3	0.0	–	–	–
N, rpm	–	–	–	3	1729	36	2	3235	0.09	2	2400	0.09	1	2100	0	3	1400	75
ρ_L, kg m^{-3}	4	2042	310	4	2042	700	5	2042	429	4	2042	310	3	2042	310	6	1844	310
μ_L, Pa s	5	0.09	5.00×10^{-5}	5	0.09	1.50×10^{-4}	6	0.09	5.00×10^{-5}	5	0.09	5.00×10^{-5}	4	0.09	5.00×10^{-5}	7	6.7×10^{-3}	5.0×10^{-5}
σ_L, N m^{-1}	6	0.077	1.20×10^{-3}	6	0.077	0.008	7	0.077	1.20×10^{-3}	6	0.074	1.20×10^{-3}	5	0.072	1.20×10^{-3}	8	0.072	1.20×10^{-3}
ρ_G, kg m^{-3}	7	194.90	0.05	7	53.86	0.05	8	53.86	0.06	7	55.27	0.05	6	55.27	0.05	9	55.17	0.05
$M_{W\text{-}Gas}$, kg kmol^{-1}				8	44	2	11	44	2	8	44	2	–	–	–	–	–	–
d_T, m	8	3.330	0.075	9	1.500	0.113	9	3.600	0.075	–	–	–	7	3.330	0.076	–	–	–
$d_{Imp.}$, m	9	1.370	0.032	10	0.5	0.05	10	1.350	0.032	–	–	–	–	–	–	–	–	–
N_{CR}, rpm	–	–	–	12	1106	30	–	–	–	–	–	–	–	–	–	–	–	–
X_W, wt.%	–	–	–	–	–	–	13	100.00	55.89	9	100	88	–	–	–	–	–	–
D_{AB}, m^2 s^{-1}	–	–	–	–	–	–	–	–	–	–	–	–	8	1.5×10^{-7}	8.4×10^{-11}	–	–	–
Gas dispersion type	10	1	0	11	1	0	–	–	–	–	–	–	–	–	–	–	–	–
ε_G	–	–	–	–	–	–	–	–	–	10	0.59	5.30×10^{-5}	9	0.54	0	–	–	–
d_S, m	–	–	–	–	–	–	–	–	–	–	–	–	10	8.9×10^{-3}	0	–	–	–
T, K	–	–	–	–	–	–	–	–	–	–	–	–	–	–	–	1	473	297
P, MPa	–	–	–	–	–	–	–	–	–	–	–	–	–	–	–	2	5.96	0.09
d_T/H	–	–	–	–	–	–	–	–	–	–	–	–	–	–	–	4	1.00	0.39
$d_{Imp.}/H_L$	–	–	–	–	–	–	–	–	–	–	–	–	–	–	–	5	0.67	0.21

Table 7
Statistical analysis of the empirical and BPNN correlations

Parameters	Regression coefficient R^2, %		Standard deviation σ, %		Average absolute relative error AARE, %	
	Empirical	BPNN	Empirical	BPNN	Empirical	BPNN
N_{CR}	96 [73]	97	14	4	7	3
Q_{GI}	70 [73]	97	50	20	35	15
a_{Wave}	92 [73]	97	5	2	3	2
ε_G	87	92	48	27	24	16
d_S	92	97	23	12	13	8
k_La	80	91	52	28	32	18

Table 8
Input variables for gas distribution and reactor type used in the BPNN correlations

Gas distribution type	Reactor mode	Values for the BPNN
Surface-aeration	SAR	0
Hollow shaft	GIR	0.5
Draft tube	GSR	1

2.2. Back-propagation neural network (BPNN) correlations

The same database (7374 experimental points) shown in Table 4 was also used to develop BPNN correlations for predicting the critical mixing speed, induced gas flow rate, wavy gas–liquid surface, gas holdup, Sauter mean bubble diameter and volumetric mass transfer coefficients for the corresponding reactor types. The transfer function used in the BPNNs was a sigmoid $(1/(1+\exp(-x))$, and the training was supervised using the gradient descent method [47]. The BPNNs developed were validated using 25% of the total number of data points and the cross validation technique [47]. Table 6 presents the input variables, architecture and weights of the constructed BPNNs for predicting N_{CR}, Q_{GI}, a_{Wave}, ε_G, d_S and k_La. Also, Table 7 shows the regression coefficient (R^2), standard deviation (σ) and average absolute relative error (AARE) for the empirical and BPNN correlations. These statistical errors prove that the developed BPNNs can predict the values of N_{CR}, Q_{GI}, a_{Wave}, ε_G, d_S and k_La with much higher accuracies than those of the empirical correlations as can be observed in Figs. 2–4. Therefore, in this study, the algorithm used for predicting these parameters was based on the BPNN correlations. It should also be mentioned that the reactor and gas dispersion mode were assigned in the BPNN correlations as shown in Table 8.

3. Algorithm for calculating the hydrodynamic and mass transfer parameters

In this study, the empirical correlations and BPNNs were used in parallel to develop the calculation algorithm, which could be employed to predict the hydrodynamic and mass transfer parameters in agitated reactors as depicted in Fig. 5.

The calculation algorithm consists of the following steps:

1. Calculate N_{CRE} for SARs, Eq. (1) or N_{CRI} for GIRs, Eq. (2), or the BPNN in Table 9.
2. If $N_{CRI} < N$, calculate Q_{GI} for GIRs, Eq. (3) or Table 10, otherwise $Q_{GI} = 0$ and the reactor is an SAR.
3. Obtain P^*/V_L in SARs, GIRs and GSRs using the empirical literature correlations given in Appendix A. If using BPNNs correlations, go to step 4.
4. Calculate ε_G, Eq. (5) for SARs, (8) for GIRs and (11) for GSRs, or Table 11.
5. Calculate d_S using Eq. (14) for SARs, (17) for GIRs and (20) GSRs, or Table 12.
6. Calculate k_La, Eqs. (23), (26) and (29) or the BPNN in Table 13.
7. Calculate a_{Wave} from Eq. (4) or the BPNN in Table 14.
8. Calculate a, Eq. (32):

$$a = \frac{6\varepsilon_G}{(1-\varepsilon_G)d_S} + a_{Wave} \tag{32}$$

9. Calculate k_L, Eq. (33):

$$k_L = \frac{k_La}{a} \tag{33}$$

It should be mentioned that a_{Wave} was used in Eq. (32) in order to take into account the effect of the wavy surface area, which can have a significant impact, particularly in small-scale agitated reactors [73].

As an example, the developed algorithm based on the BPNN correlations was used to predict the effect of liquid viscosity, mimicking the evolution of the hydrogenation process, and hydrogen mole fraction in the gaseous feed mixture ($H_2 + N_2$) to the reactor on the hydrodynamics and mass transfer parameters in soybean oil hydrogenation process conducted in a large-scale gas-sparging agitated reactor. A brief background on the vegetable oil hydrogenation processes and the simulation results are given in the following.

4. Results and discussion

The hydrogenation of vegetable oils, such as soybean oil, is a key process in the fat industry due to its applications in the production of frying fats, margarine and shortenings [78,79]. The purpose of this process is to increase the melting point of the oil, increase its stability to oxidation, enhance its frying properties and improve its solidification characteristics [78,80]. In order to obtain these properties, the double bonds along the unsaturated triglyceride chains are selectively saturated during the hydrogenation reaction [78,80]. The industrial hydrogenation

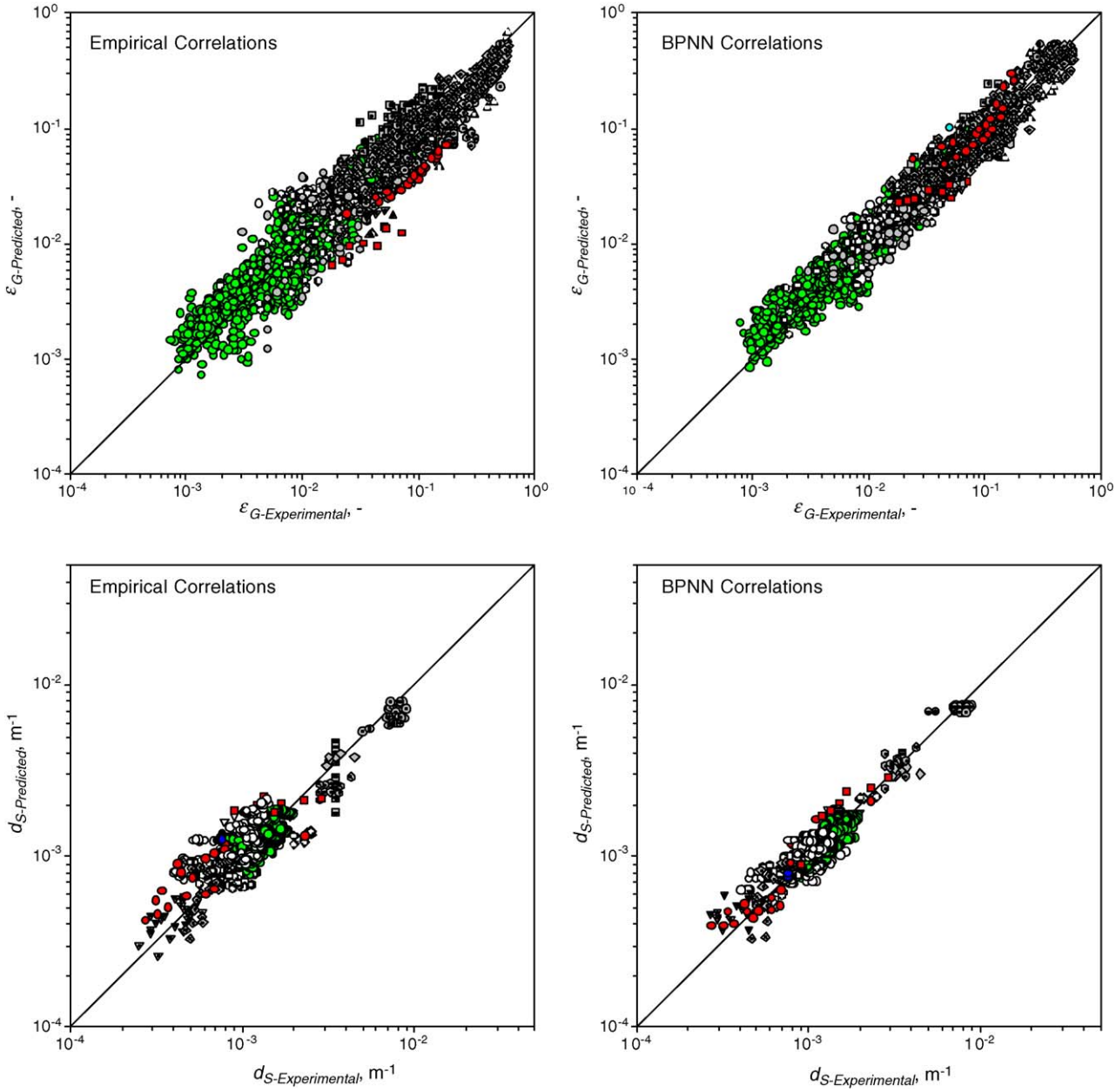

Fig. 3. Comparison between experimental and predicted ε_G and d_S values using empirical and BPNN correlations.

Table 9
Architecture, weights of the N_{CR} BPNN correlation

	1	2	3	4	5	6	7	8	9	10
First hidden layer weights $u_{i,j}$										
1	8.35	26.78	−30.16	2.63	1.72	−5.37	0.54	3.64	−1.90	−13.24
2	−28.29	−33.32	60.17	−4.83	4.48	7.00	−0.73	50.43	−69.38	32.63
3	−12.15	34.83	−80.39	6.31	−7.04	−4.18	0.82	−55.17	60.85	0.24
4	4.52	34.25	−73.91	−4.10	0.98	−3.50	−0.54	81.09	28.72	−3.49
5	−6.21	−42.45	51.52	1.45	0.92	8.78	−2.19	−11.24	1.59	13.96
6	−1.70	−27.57	−5.17	3.74	−1.58	−6.71	2.62	11.16	−20.47	2.79
7	−14.74	−29.14	−44.81	3.12	−6.13	−2.07	1.28	20.15	−23.49	1.78
8	−6.97	−6.54	−33.78	1.41	−0.68	−3.43	1.86	7.65	−10.75	0.91
Bias of first hidden layer $u_{0,i}$	4.85	−3.93	3.75	6.92	−11.05	5.52	5.01	9.85		
Output layer weights w_i	14.02	8.42	17.05	−33.35	4.38	4.07	−16.60	−4.15		
Bias of output neuron w_0	19.89									

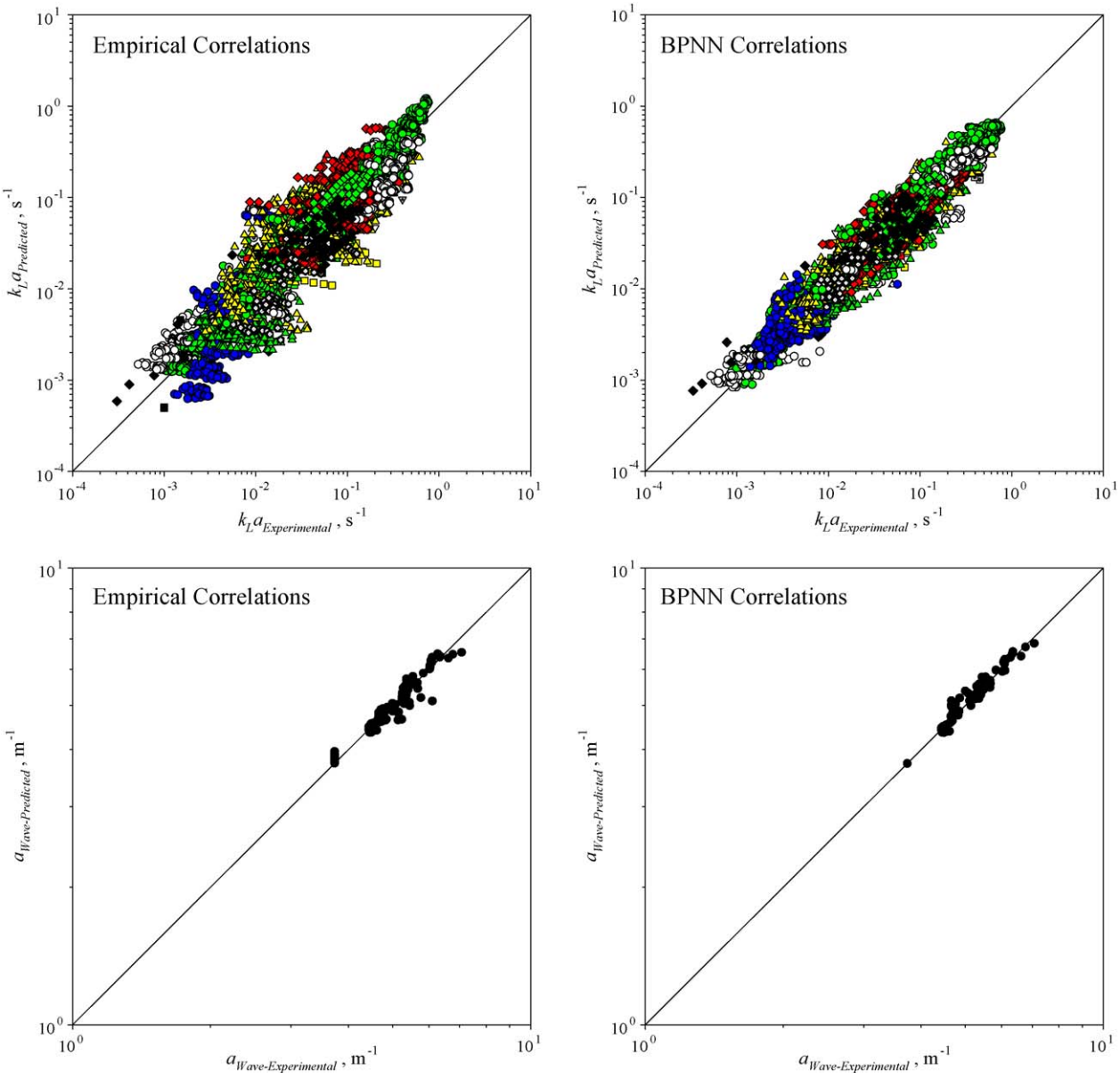

Fig. 4. Comparison between experimental and predicted $k_L a$ and a_{Wave} values using empirical and BPNN correlations.

Table 10
Architecture, weights of the Q_{GI} BPNN correlation

	1	2	3	4	5	6	7	8	9	10	11	12
First hidden layer weights $u_{i,j}$												
1	−14.15	8.50	−7.38	−4.82	−7.26	−11.92	−2.60	4.68	2.29	−0.89	22.17	14.43
2	−6.31	0.83	4.64	−9.98	−3.71	1.32	2.13	3.44	7.23	4.39	−9.67	20.24
3	−9.90	9.56	−7.69	−3.34	−17.75	−0.80	0.05	2.85	4.80	−6.12	5.86	−0.30
4	5.19	−5.30	−16.27	0.81	−16.10	0.65	1.44	0.88	0.96	2.20	−0.89	13.58
5	18.75	−14.83	2.10	8.76	0.52	−0.92	2.20	0.07	−8.23	0.37	−3.11	0.56
6	−14.27	3.30	−9.12	−3.73	−16.10	−5.30	−0.29	5.63	2.65	8.07	10.14	7.89
7	−47.58	1.04	−5.45	−26.94	−21.08	18.79	0.37	9.25	−47.74	6.08	−11.01	11.30
8	−0.66	9.05	−8.41	−1.13	0.97	−12.44	−0.11	−3.41	−12.49	−6.43	−3.67	0.59
Bias of first hidden layer $u_{0,i}$	−13.35	2.35	−0.48	−4.77	−1.94	−4.33	−13.89	5.79				
Output layer weights w_i	−4.95	8.09	−5.90	−7.91	−2.67	8.75	−28.30	−7.14				
Bias of output neuron w_0	−6.36											

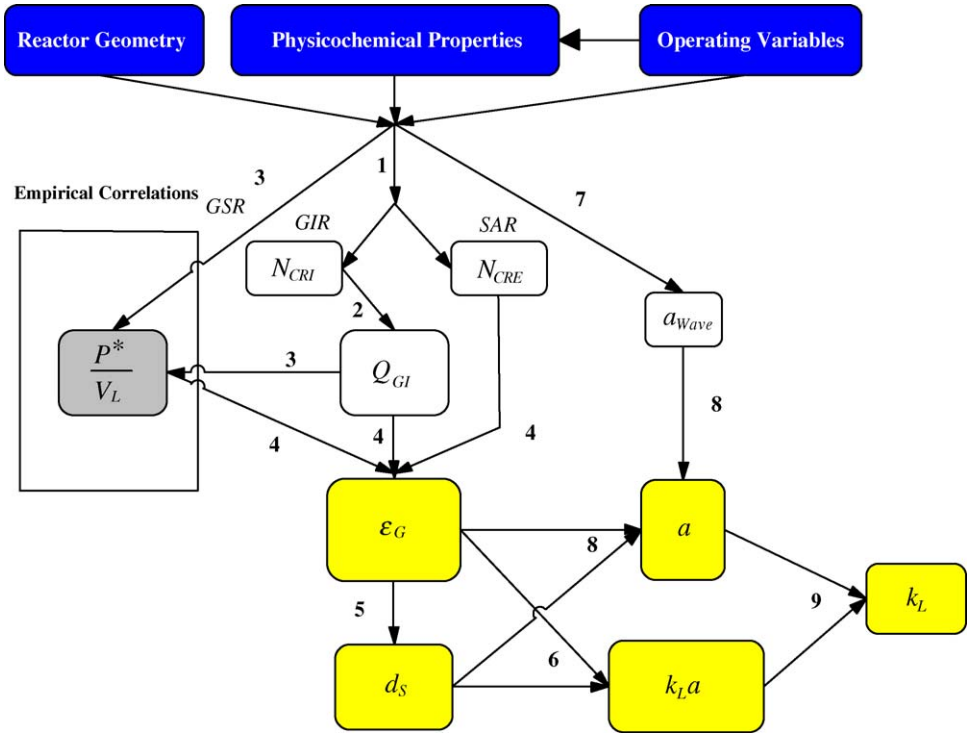

Fig. 5. Calculation algorithm for the hydrodynamic and mass transfer parameters using the empirical and BPNN correlations.

Table 11
Architecture, weights of the ε_G BPNN correlation

	1	2	3	4	5	6	7	8	9	10	11	12	13
First hidden layer weights $u_{i,j}$													
1	−18.65	13.91	−9.73	−2.87	2.46	−34.93	−10.02	−4.88	32.85	6.69	0.57	−17.83	3.04
2	−17.66	14.99	3.83	5.82	6.51	−0.99	1.57	6.64	0.81	6.17	1.14	5.55	−1.68
3	−1.52	1.94	0.90	−22.86	−5.65	0.19	3.81	3.09	6.38	−0.99	−3.10	−2.95	2.81
4	−0.09	7.78	−12.13	−4.16	2.46	4.34	13.73	−2.41	10.69	−0.19	−0.92	−4.79	−0.79
5	4.33	−1.52	−7.36	3.77	−1.03	−0.29	−3.72	1.61	−4.96	3.77	1.95	−4.53	0.61
6	1.71	−10.63	−1.31	−29.96	4.46	−1.36	−7.26	−9.25	−0.03	−5.51	9.98	−16.02	1.86
7	2.36	5.02	−0.81	6.96	7.03	−0.66	4.62	−2.82	16.71	7.23	−0.42	−12.60	−2.28
8	−14.89	10.62	−10.55	3.45	0.73	−5.76	−8.67	−5.38	−15.38	1.08	0.67	−9.04	1.13
9	−15.53	10.15	0.49	−6.09	11.92	1.88	6.77	−1.01	1.47	5.21	−2.00	7.93	−2.56
10	2.97	−2.43	17.06	19.45	5.69	−2.78	1.32	4.15	−2.59	31.89	0.31	22.51	−1.76
Bias of first hidden layer $u_{0,i}$	−2.38	4.84	−5.78	−0.39	−5.13	−0.59	−5.00	0.72	0.10	−1.09			
Output layer weights w_i	13.01	2.72	−8.58	6.90	8.73	−0.88	3.78	−12.50	−2.65	−3.76			
Bias of output neuron w_0	−5.54												

Table 12
Architecture, weights of the d_S BPNN correlation

	1	2	3	4	5	6	7	8	9	10
First hidden layer weights $u_{i,j}$										
1	−1.20	−2.69	−4.12	0.34	57.32	−0.29	1.11	−1.82	−1.33	5.16
2	0.80	−1.39	3.99	−19.39	7.16	9.37	0.84	−1.84	−0.58	6.67
3	−29.44	−3.44	24.54	0.42	−4.01	−3.18	0.08	1.05	0.15	−1.13
4	−1.75	−1.80	37.87	24.52	23.66	−8.15	−0.75	0.59	0.83	−22.79
5	12.89	−1.24	10.97	−90.95	66.59	32.98	0.18	−0.94	0.68	−25.47
6	0.43	0.71	−4.85	17.89	−27.40	14.11	−0.04	−12.44	−6.12	−2.02
Bias of first hidden layer $u_{0,i}$	6.58	1.63	16.31	1.47	9.83	−4.44				
Output layer weights w_i	−7.70	3.84	−1.42	2.63	−1.19	−2.09				
Bias of output neuron w_0	5.57									

Table 13
Architecture, weights of the $k_L a$ BPNN correlation

	1	2	3	4	5	6	7	8	9	10
First hidden layer weights $u_{i,j}$										
1	2.88	4.87	−0.58	−9.02	5.98	−0.17	−3.67	−0.67	−7.76	−22.32
2	−2.09	9.11	3.01	8.08	−9.03	−0.09	−29.15	−18.32	3.53	−5.85
3	9.81	−19.61	0.31	−17.34	−5.20	6.11	−0.32	−9.38	13.21	−20.79
4	−1.20	−9.28	−15.05	8.45	1.68	−1.56	1.47	−4.67	1.07	1.38
5	−9.35	2.52	6.38	−24.46	−1.51	−0.18	−7.52	3.38	−5.27	7.29
6	−2.07	−12.16	38.68	−10.52	−15.93	−1.72	−0.70	−6.62	−6.22	0.68
7	−0.10	7.14	−24.48	−22.50	7.56	−1.97	−3.66	−8.07	12.88	−3.50
8	−9.56	6.55	−11.73	0.70	9.45	−6.24	0.58	8.97	81.82	−0.49
9	0.95	5.94	−5.27	25.29	0.95	0.48	−3.14	−9.46	4.65	36.31
10	1.78	−7.27	11.60	25.96	−19.65	−0.46	−21.74	1.35	11.97	3.81
Bias of firsst hidden layer $u_{0,i}$	0.82	4.52	−2.16	5.09	0.72	−3.21	1.80	5.67	−1.96	−3.57
Second hidden layer weights $v_{i,j}$										
1	1.27	−9.88	−0.42	1.58	−1.63	16.16	4.88	−3.03	8.32	5.63
2	−7.05	−2.78	0.72	20.23	−19.60	1.37	9.44	−1.67	6.20	−26.30
3	16.65	−12.39	−2.78	4.43	11.46	−8.95	−9.19	0.46	21.81	22.59
4	7.31	−1.24	−5.42	2.73	−2.78	9.01	−3.16	−7.21	2.29	14.68
5	7.55	−4.91	−0.20	5.70	1.45	−5.28	−2.31	−0.10	12.16	4.73
6	1.75	−1.59	0.94	−1.45	1.51	4.43	−17.00	1.17	−0.05	−8.04
7	4.46	3.24	−1.33	7.23	4.54	−7.43	0.51	−1.09	1.77	−0.62
8	−8.50	−0.83	−22.08	6.93	−3.57	7.13	−11.62	−21.44	−5.45	−22.50
Bias of second hidden layer $v_{0,i}$	−10.66	−12.17	−21.03	−7.88	−14.04	−1.62	−9.50	18.08		
Output layer weights w_i	2.61	−1.25	−1.29	−3.12	2.51	−2.90	−3.51	−10.20		
Bias of output neuron w_0	1.99									

of soybean oil is usually carried out in a three-phase agitated reactor where gaseous hydrogen, liquid soybean oil and solid Ni- or Pd-based catalyst are used [78,80]. The operating conditions of the process range from 393 to 473 K, 1 to 5 bar and 0.01 to 0.1 wt.% catalyst [81], and is usually carried out in GSRs operating in a batch mode [13]. The capacity of the commercial soybean oil hydrogenation reactors typically varies between 5 and 30,000 kg; and in the United States, the hydrogenation of soybean oil process is referred to as the Normann process [82].

In the hydrogenation process, the knowledge of the iodine value (I.V.) is essential as it characterizes the number of double bonds of the oil. The I.V. value is related to the amount of hydrogen consumed, and thus the control of the amount of hydrogen in the gaseous feed to the reactor is of prime importance for the quality and properties of the oil as well as for the process economics. Topallar et al. [83] reported that a drop of I.V. value from 131.7 to 82.4 during vegetable oil hydrogenation can increase the oil viscosity by a factor of 1.5–1.7. Similar findings were reported by Fillion [13], who emphasized the effect of oil viscosity on the process design. Also, due to the explosive nature of hydrogen, the commercial reactor could be safely operated with a ($H_2 + N_2$) mixture, which could have a strong impact on the process hydrodynamics and mass transfer [13].

In this study, the effects of liquid-phase viscosity and hydrogen mole fraction in the gaseous feed ($H_2 + N_2$) to the reactor on the hydrodynamic and mass transfer parameters for soybean oil hydrogenation in a large-scale gas-sparging agitated reactor were predicted using the developed algorithm based on the BPNN correlations. The reactor used in the simulation was: 2.5 m (inside diameter), 5 m height, 7.8125 m^3 liquid volume and about 7000 kg soybean oil capacity at room temperature. Details of the reactor geometry, operating conditions and gas–liquid physicochemical properties used as input to the BPNNs are given in Table 15. It should be mentioned that Fillion [13] reported no effects of catalyst loading on the hydrodynamic and mass transfer parameters in soybean oil hydrogenation if the Ni-wt.% were

Table 14
Architecture, weights of the a_{Wave} BPNN correlation

	1	2	3	4	5	6	7	8	9
First hidden layer weights $u_{i,j}$									
1	1.73	14.79	−3.45	−5.05	7.50	2.72	8.19	12.41	−6.86
2	−7.48	7.36	−0.88	33.75	−23.57	−14.92	7.99	−7.91	−6.53
3	8.31	3.18	−1.56	−15.79	−10.94	20.27	2.21	26.92	−6.14
4	4.56	−11.59	1.52	−7.97	−2.97	13.38	0.84	8.53	14.59
Bias of first hidden Layer $u_{0,i}$	−1.48	10.15	−10.95	1.47					
Output layer weights w_i	−7.50	−11.14	−21.93	9.98					
Bias of output neuron w_0	4.22								

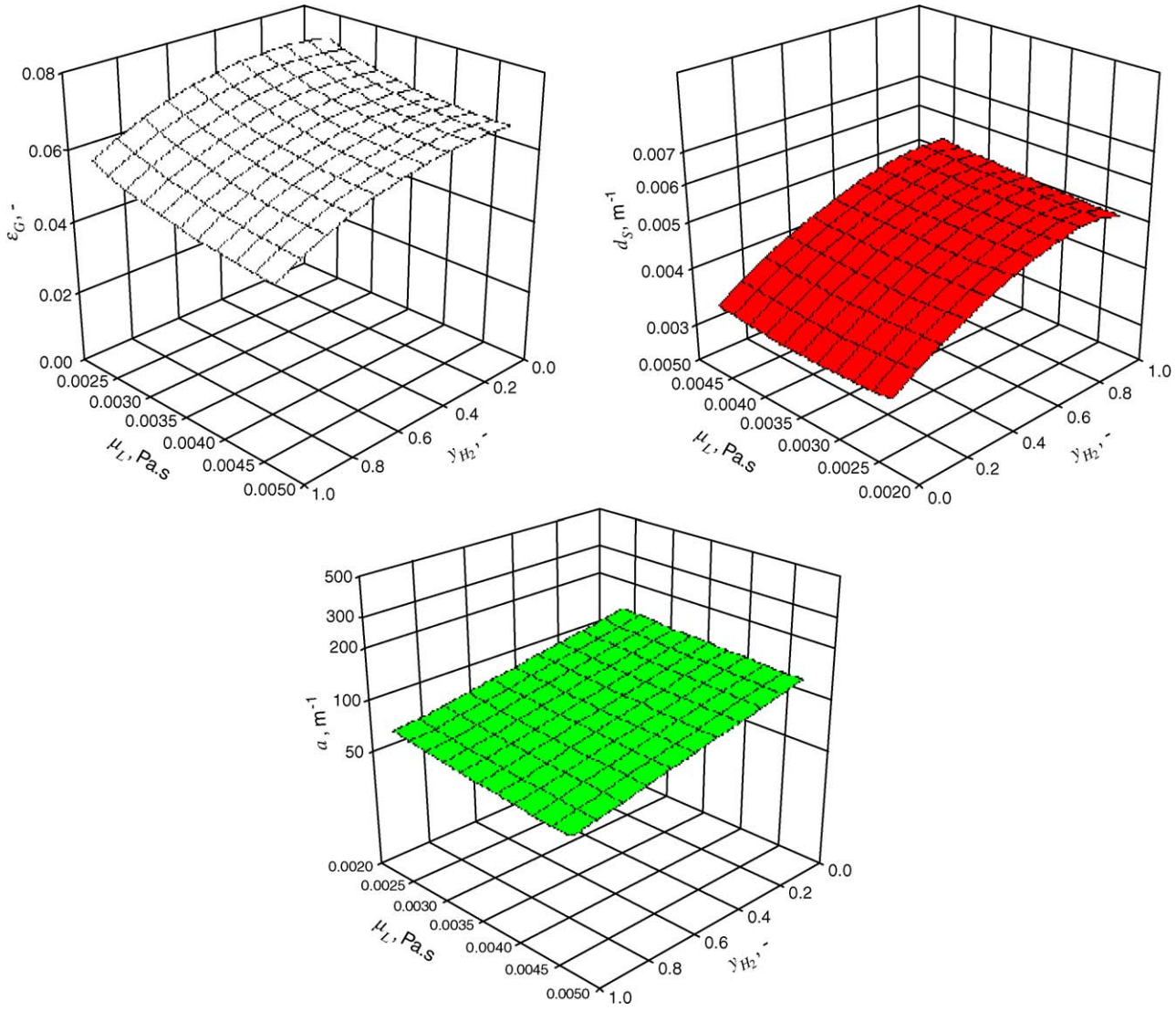

Fig. 6. Effect of liquid viscosity and y_{H_2} on ε_G, d_S and a for the soybean process using BPNN correlations.

less than 0.16, and accordingly the use of the present algorithm developed for gas–liquid system under the conditions given in Table 15 can be justified.

Fig. 6 shows that increasing liquid-phase viscosity from 0.0023 to 0.0047 at constant pressure (P) = 0.5 MPa, temperature (T) = 473 K, and superficial gas velocity (U_G) = 0.04 m s^{-1}, decreases the total gas holdup (ε_G) by 15% within the H_2 mole fraction range used (0–1). This decrease of the gas holdup with increasing liquid-phase viscosity could be due to the increase of gas bubbles coalescence; and is in agreement with the findings by Rushton and Bimbinet [14], Loiseau [50] and Fillion [13]. Increasing liquid-phase viscosity also increases the Sauter mean bubble diameter (d_S) from 0.0049 to 0.0053 m, which clearly indicates the increase of the gas bubbles coalescence with increasing liquid-phase viscosity.

Fig. 6 also shows that increasing the hydrogen mole fraction (y_{H_2}) from 0 to 1 at constant P = 0.5 MPa, T = 473 K, and U_G = 0.04 m s^{-1} within the soybean oil range of liquid viscosity range employed (0.0023–0.0047 Pa s) decreases the gas holdup by up to 20%. This decrease of ε_G can be related to the decrease of gas density (i.e. the gas momentum) with increasing the H_2 mole fraction in the gas mixture, which is in accordance with available literature findings [5,9,13]. Increasing the H_2 mole fraction, on the other hand, appears to slightly increase the Sauter mean diameter from 0.0035 to 0.0053 m, which can be attributed to the increase of the probability of gas bubbles coalescence with decreasing the gas momentum. This behavior of d_S is in agreement with the results by Fillion [13] who found that under similar operating conditions H_2 bubble sizes were larger than those of N_2 in soybean oil, since under the same pressure, temperature and superficial gas velocity, N_2 would exhibit greater momentum than H_2. Thus, the decrease of the gas holdup and the increase of the Sauter mean bubble diameter with increasing either the liquid-phase viscosity or the H_2 mole fraction obviously lead to the decrease of the gas–liquid interfacial area, a according to Eq. (32), as can be seen in Fig. 6.

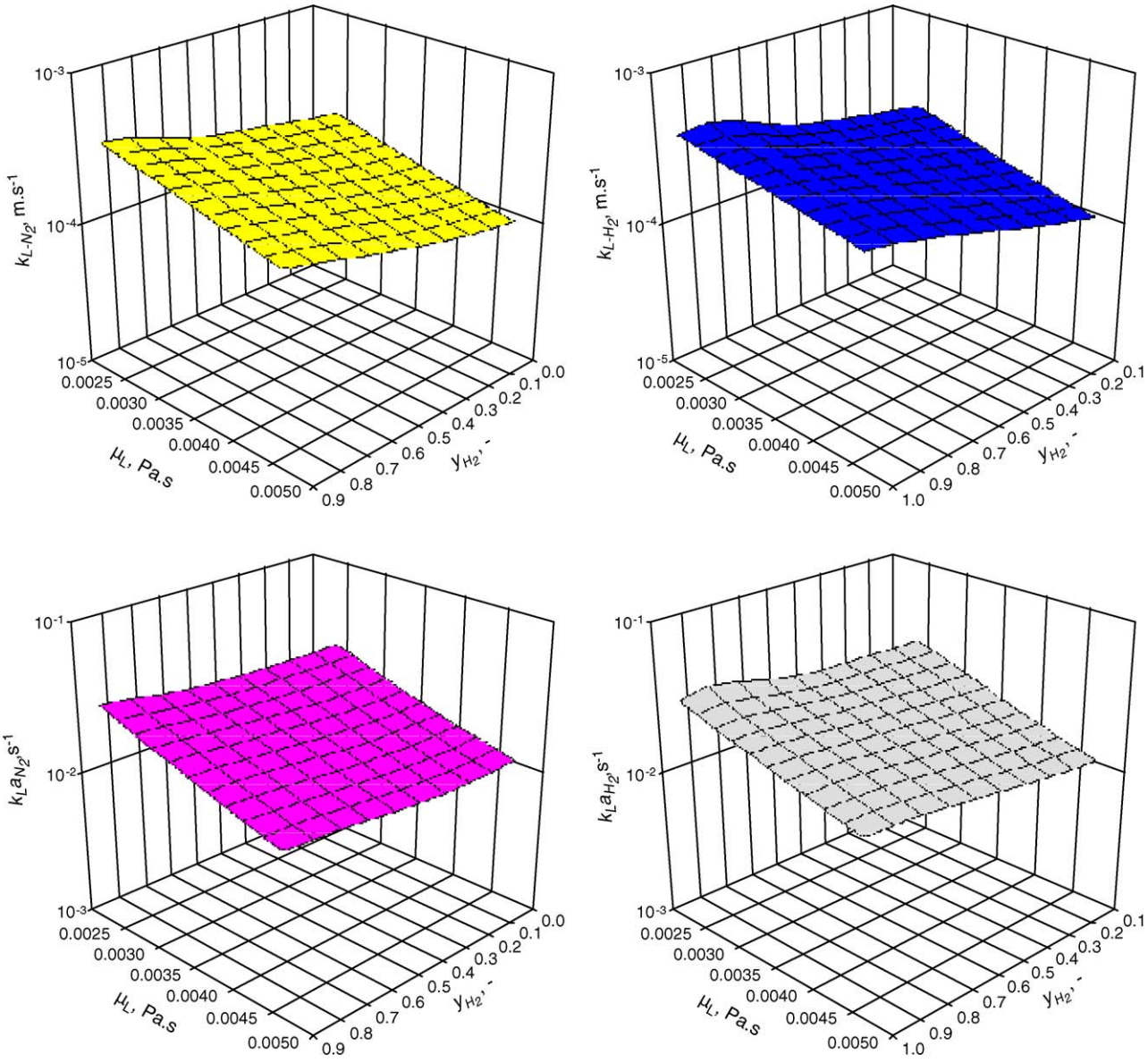

Fig. 7. Effect of liquid viscosity and y_{H_2} on k_L and $k_L a$ of N_2 and H_2 for the soybean process using BPNN correlations.

Increasing the liquid-phase viscosity is supposed to decrease the gas diffusivity in the liquid-phase (D_{AB}) following the modified Wilke and Chang's equation proposed by Fillion [13], and since the mass transfer coefficient (k_L) is proportional to the D_{AB} to the power 0.5 and 1.0 according to the penetration theory and two-film model, respectively, the k_L values for H_2 and N_2 are expected to decrease with increasing the liquid-phase viscosity. The increase of the Sauter mean bubble diameter with increasing liquid-phase viscosity, however, is expected to increase the mass transfer coefficient (k_L), since k_L was reported to be directly proportional to d_S [84,85]. It appears that under the operating range studied, the decrease of k_L due to the increase of liquid-phase viscosity is stronger than its increase due to the increase of the Sauter mean bubble diameter, leading to the observed decrease of k_L as shown in Fig. 7. On the other hand, increasing the H_2 mole fraction within the liquid-phase viscosity range (0.0023–0.47 Pa s) was found to increase the Sauter mean bubble diameter, which was expected to increase the mass transfer coefficients, k_L for H_2 and N_2 according to literature findings [84,85] and as can be seen in Fig. 7.

Thus, from the above discussion increasing the liquid viscosity decreased the gas–liquid interfacial area and the mass transfer coefficients for H_2 and N_2, and consequently the volumetric mass transfer coefficients ($k_L a$) for both gases should decrease with increasing the liquid-phase viscosity as can be clearly seen in Fig. 7. Actually, in this figure, the values of $k_L a_{H_2}$ and $k_L a_{N_2}$ appear to decrease by 60% with increasing liquid-phase viscosity from 0.0023 to 0.0047 Pa s within the H_2 mole fraction range used. The decrease of the gas–liquid interfacial area and the increase of the mass transfer coefficient (k_L) with increasing the H_2 mole fraction as discussed above could

Table 15
Reactor geometry, operating conditions and physical properties of the GSR simulating the soybean oil process

System	$H_2 + N_2$-Soybean Oil-0.16 wt.% Ni	
Reactor and sparger geometry	d_T, m	2.5
	$d_{Imp.}$, m	$d_T/3$
	H, m	$2\,d_T$
	H_L, m	$d_T/3$
	$n_{Imp.}$	3
Operating variables	T, K	473
	P, MPa	0.5
	U_G, m s^{-1}	0.04
	N, Hz	1.25
	X_W, wt.%	100
	y_{H_2}	0–1
System physical properties	ρ_L, kg m^{-3}	800
	μ_L, Pa s	2.33×10^{-3}–4.66×10^{-3}
	σ_L, N m^{-1}	0.0247
	ρ_G, kg m^{-3}	3.56–0.25
	$D_{AB\text{-}H_2}$, m^2 s^{-1}	1.24×10^{-8}–1.88×10^{-8}
	$D_{AB\text{-}N_2}$, m^2 s^{-1}	1.00×10^{-8}–1.52×10^{-8}

lead to the increase or decrease of the volumetric mass transfer coefficients (k_La) for both gases. Fig. 7, however, shows that $k_La_{H_2}$ and $k_La_{N_2}$ values only increase by 25% with increasing the H_2 mole fraction within the liquid-phase viscosity used (0.0023–0.0047 Pa s). This indicates that the mass transfer coefficients (k_L) for both gases have a stronger influence on their corresponding k_La values than the gas–liquid interfacial area within the operating conditions used.

Fig. 7 also shows that, under similar conditions, k_La values for H_2 in soybean oil when using the gaseous mixture ($H_2 + N_2$) are about 25% lower than those obtained for H_2 (as a single-component). This finding is important for the design of GSRs; and is in good agreements with the 5–15% decrease of the H_2 reaction rate measured by Fillion [13] while hydrogenating soybean oil using different ($N_2 + H_2$) ratios. In addition, the figure illustrates that k_L values for H_2 are consistently greater than those of N_2, which can be related to the fact that the diffusivity of H_2 in soybean oil is always greater than that of N_2 according to the modified Wilke and Chang's equation by Fillion [13].

5. Conclusions

A large number of data points (7374) on the hydrodynamic and mass transfer parameters obtained in our laboratories and from the literature in ARs, covering different reactor sizes and operating conditions were used to develop novel empirical and neural network (BPNN) correlations which were employed to construct a simple algorithm for predicting these parameters under industrial conditions. Due to their high confidence levels and flexibility, the developed BPNN models were incorporated in the algorithm, which was then used to predict the effects of viscosity and hydrogen mole fraction in the feed gas ($H_2 + N_2$) on the hydrodynamic and mass transfer parameters for H_2 and N_2 in soybean oil hydrogenation process conducted in a large-scale GSR (2.5 m i.d. and 5 m height).

The algorithm predictions showed that increasing the liquid-phase viscosity decreased the ε_G and increased d_S, resulting in a decrease of a. The decrease of the gas holdup with increasing the liquid-phase viscosity was related to the increase of gas bubble coalescence under these conditions. Increasing the liquid-phase viscosity, however, decreased k_L as well as k_La values for both H_2 and N_2 within the range H_2 mole fraction (0–1) used. This k_L behavior indicated that the effect of viscosity on k_L is more significant than that of d_S. The predictions also showed that increasing the H_2 mole fraction in the feed to the reactor decreased ε_G and increased d_S, resulting in a decrease of a and an increase of k_L as well as k_La for both H_2 and N_2 within the range of liquid-phase viscosity used (0.0023–0.0047 Pa s). The decrease of the gas holdup with increasing the H_2 mole fraction in the feed gas was attributed to the decrease of the density (momentum) of the gas mixture. The increase of k_L values with increasing the H_2 mole fraction in the feed gas was related to the increase of d_S, since k_L was reported to be directly proportional to d_S. The predicted k_La values indicted that the mass transfer behavior in the gas-sparging reactor proposed in this study for soybean oil hydrogenation was controlled by the mass transfer coefficient, k_L. Also, under similar conditions, k_La values for H_2 in soybean oil when using the gaseous mixture ($H_2 + N_2$) were found to be about 25% lower than those obtained for H_2 (as a single-component), and k_L values for H_2 were consistently greater than those of N_2 within the ranges of the operating conditions used.

It should be mentioned that although the developed algorithm appears to be a viable tool for predicting the hydrodynamic and mass transfer parameters in large-scale ARs used in commercial processes, the accuracy of such predictions could be further improved by diversifying and expanding the experimental data bank used, particularly with large-scale reactors, operating under actual industrial conditions.

Appendix A

The power input per unit volume in SARs was calculated as follows:

$$\frac{P^*_{SAR}}{V_L} = \frac{N_P \times d^5_{Imp.} \times \rho_L \times N^3}{V_L} \tag{A.1}$$

N_P, the power number, is function of the impeller type and geometry as well as the Reynolds number [3].

The gassed power input per unit liquid volume in GIRs equipped with a hollow shaft was calculated from Heim et al. [20]:

$$\frac{P^*_{GIR}}{V_L} = \frac{P^*_{SAR}}{V_L} \times \left(1 - \exp\left(A + \frac{a_1}{\sqrt{Fr}} + a_2 Re\right)\right) \tag{A.2}$$

A, a_1 and a_2 are constants which are function of the impeller design.

For GIRs equipped with a draft tube, the expression developed by Saravanan et al. [86] was used:

$$\frac{P^*_{GIR}}{V_L} = \frac{\rho_L W N^3 (d_{Imp.}/2)^4}{V_L}\left(C^*_{DO} - C^*_{DY}\left(1 - \frac{1}{\Phi F_S}\right)^3\right) + \frac{\tau_{rg} 2\pi N}{V_L} \quad (A.3)$$

W is the impeller width, C^*_{DO} and C^*_{DY} the impeller drag coefficients in the gas–liquid dispersion conveying and central zone, respectively, Φ the vortexing constant, F_S the Froude number based on submergence and τ_{rg} is the torque representing the effect of recycled fluid on the power input.

In GSRs, the power input per unit volume was calculated from Loiseau et al. [15]:

$$\frac{P^*_{GSR}}{V_L} = \frac{A}{V_L} \times \left(\frac{P^*_{SAR} N d^3_{Imp.}}{Q^{0.56}_G}\right)^B \quad (A.4)$$

A and B are constants.

Also, the power of the sparged gas from the compressor was calculated according to Shridhar and Potter [9] as:

$$U_G \rho_L g \quad (A.5)$$

References

[1] J.C. Charpentier, Mass Transfer Rates in Gas–Liquid Absorbers and Reactors, Advances in Chemical Engineering, vol. 11, Academic Press, 1981.

[2] E.H. Stitt, Alternative multiphase reactors for fine chemicals. A world beyond stirred tanks? Chem. Eng. J. 90 (2002) 47–60.

[3] Z. Tekie, Mass transfer and modeling of the liquid-phase cyclohexane oxidation process in agitated reactors, Ph.D. dissertation, University of Pittsburgh, 1997.

[4] P.L. Mills, R.V. Chaudhari, Reaction engineering of emerging oxidation processes, Catal. Today 48 (1999) 17–29.

[5] R. Lemoine, B.I. Morsi, Hydrodynamic and mass transfer parameters in agitated reactors, Part II: gas-holdup, Sauter mean bubble diameters, volumetric mass transfer coefficients, gas–liquid interfacial areas, and liquid-side mass transfer coefficients, Int. J. Chem. Reac. Eng. 3 (2005) A20.

[6] T. Vermeulen, G.M. Williams, G.E. Langlois, Interfacial area in liquid–liquid and gas–liquid agitation, Chem. Eng. Progr. 51 (2) (1955) 85F–94F.

[7] P.H. Calderbank, Physical rate processes in industrial fermentation. Part I: the interfacial area in gas–liquid contacting with mechanical agitation, Trans. Inst. Chem. Eng. 36 (1958) 442–459.

[8] D.N. Miller, Scale-up of agitated vessels gas–liquid mass transfer, AIChE J. 20 (3) (1974) 445–453.

[9] T. Shridhar, O.E. Potter, Gas holdup and bubble diameters in pressurized gas–liquid stirred vessels, Ind. Eng. Chem. Fundam., 19 (1980) 21–26.

[10] G.A. Hughmark, Power requirements and interfacial area in gas–liquid turbine agitated systems, Ind. Eng. Chem. Process Des. Dev. 19 (1980) 638–641.

[11] M. Matsumura, H. Sakuma, T. Yamagata, J. Kobayashi, Performance of oxygen transfer in a new gas entraining fermentor, J. Ferment. Technol. 60 (6) (1982) 551–563.

[12] R. Parthasarathy, G.J. Jameson, N. Ahmed, Bubble breakup in stirred vessels-predicting the Sauter mean diameter, Trans. Inst. Chem. Eng. 69 (A) (1991) 295.

[13] B. Fillion, Modeling of soybean oil hydrogenation process, Ph.D. dissertation, University of Pittsburgh, 2001.

[14] J.H. Rushton, J-J. Bimbinet, Holdup and flooding in air liquid mixing, Can. J. Chem. Eng. 46 (1968) 16–21.

[15] B. Loiseau, N. Midoux, J.-C. Charpentier, Some hydrodynamics and power input data in mechanically agitated gas–liquid contactors, AIChE J. 23 (1977) 931.

[16] M. Matsumura, H. Masunaga, K. Haraya, J. Kobayashi, Effect of gas entrainment on the power requirement and gas holdup in a aerated stirred tank, J. Ferment. Technol. 56 (2) (1978) 128–138.

[17] M.M. Lopes de Feigueiredo, P.H. Calderbank, The scale-up of aerated mixing vessels for specified oxygen dissolution rates, Chem. Eng. Sci. 34 (1979) 1333–1338.

[18] D.X. He, S.H. Chiang, G.E. Klinzing, Operating characteristics of a gas/liquid contactor using gas-inducing turbine, J. Chin. Inst. Chem. Eng. 22 (1991) 321–328.

[19] A.M. Al Taweel, Y.H. Cheng, Effect of surface tension on gas/liquid contacting in a mechanically-agitated tank with Stator, Trans. I. Chem. E. 73 (A) (1995) 654–659.

[20] A. Heim, A. Kraslawski, E. Rzyski, J. Stelmach, Aeration of bioreactors by self-aspirating impellers, Chem. Eng. J. 58 (1995) 59–63.

[21] K. Wichterle, Free level effect on the impeller power input in baffled tanks, Collect. Czech. Chem. Commun. 60 (1995) 1274–1280.

[22] K. Saravanan, J.B. Joshi, Fractional gas hold-up in gas inducing type of mechanically agitated contactors, Can. J. Chem. Eng. 74 (1996) 16–30.

[23] T. Murugesan, Dispersed phase hold-up in mechanically agitated gas–liquid contactors, J. Chem. Technol. Biotechnol. 72 (1998) 221–226.

[24] M. Matsumura, H. Masunaga, J. Kobayashi, A correlation for flow rate of gas entrained from free surface of aerated stirred tank, J. Ferment. Technol. 55 (4) (1977) 388–400.

[25] R.S. Albal, Y.T. Shah, N.L. Carr, A.T. Bell, Mass transfer coefficients and solubilities for hydrogen and carbon monoxide under fischer-tropsch conditions, Chem. Eng. Sci. 39 (1984) 905–907.

[26] C.W. Robinson, C.R. Wilke, Simultaneous measurement of interfacial area and mass transfer coefficients for a well-mixed gas dispersion in aqueous electrolyte solutions, AIChE J. 20 (2) (1974) 285–294.

[27] J.F. Perez, O.C. Sandall, Gas absorption by non-newtonian fluids in agitated vessels, AIChE J. 20 (1974) 770.

[28] L. Bern, J.O. Lidefelt, N.-H. Schoon, Mass transfer and scale-up in fat hydrogenation, J. Am. Oil Chem. Soc. 53 (1976) 463–466.

[29] J.B. Joshi, M.M. Sharma, Mass transfer and hydrodynamic characteristics of gas inducing type of agitated contactors, Can. J. Chem. Eng. 55 (1977) 683–695.

[30] M. Matsumura, H. Masunaga, J. Kobayashi, Gas absorption in an aerated stirred tank at high power input, J. Ferment. Technol. 57 (2) (1979) 107–116.

[31] M. Kara, An experimental study of hydrogen mass transfer rate in liquids hydrocarbons at high temperatures and pressures, Ph.D. dissertation, University of Pittsburgh, 1981.

[32] S.B. Sawant, J.B. Joshi, V.G. Pangarkar, R.D. Mhaskar, Mass transfer and hydrodynamic characteristics of the denver type of flotation cells, Chem. Eng. J. 21 (1981) 11–19.

[33] H. Judat, Gas/liquid mass transfer in stirred vessels—a critical review, Ger. Chem. Eng. 5 (1982) 357.

[34] B.M. Karandikar, B.I. Morsi, Y.T. Shah, N.L. Carr, Effect of water on the solubility and mass transfer coefficient of gases in a heavy fraction of Fischer-Tropsch products, Can. J. Chem. Eng. 65 (1987) 973–981.

[35] G.F. Versteeg, P.M.M. Blauwhoff, W.P.M. van Swaaij, The effect of diffusivity on gas–liquid mass transfer in stirred vessels experiments at atmospheric and elevated pressures, Chem. Eng. Sci. 42 (1987) 1103–1119.

[36] M.-Y. Chang, Mass transfer characteristics of gases in aqueous and organic liquids and slurries at elevated pressures and temperatures in agitated reactors, Ph.D. dissertation, University of Pittsburgh, 1991.

[37] H. Hichri, A. Accary, J. Andrieu, Kinetics and slurry-type reactor modeling during catalytic hydrogenation of *o*-cresol on Ni/SiO_2, Chem. Eng. Process. 30 (1991) 133–140.

[38] E. Dietrich, C. Mathieu, H. Delmas, J. Jenck, Raney-nickel catalysed hydrogenations: gas–liquid mass transfer in gas-induced stirred slurry reactors, Chem. Eng. Sci. 47 (1992) 3597–3604.

[39] N. Koneripalli, Z. Tekie, B.I. Morsi, M.-Y. Chang, Mass transfer characteristics of gases in methanol and ethanol under elevated pressure and temperature, Chem. Eng. J. 54 (1994) 63–77.
[40] T.I. Mizan, J. Li, B.I. Morsi, M.-Y. Chang, E.E. Maier, C.P.P. Singh, Solubilities and mass transfer coefficients of gases in liquid propylene in a surface-aeration agitated reactor, Chem. Eng. Sci. 49 (1994) 821–830.
[41] H. Wu, An issue on applications of a disk turbine for gas–liquid mass transfer, Chem. Eng. Sci. 50 (17) (1995) 2801–2811.
[42] M. Yoshida, A. Kitamura, K. Yamagiwa, A. Ohkawa, Gas hold-up and volumetric oxygen transfer coefficient in an aerated agitated vessel without baffles having forward–reverse rotating impellers, Can. J. Chem. Eng. 74 (1996) 31–39.
[43] Z. Tekie, J. Li, B.I. Morsi, M. -Y. Chang, Gas–liquid mass transfer in cyclohexane oxidation process using gas-inducing and surface-aeration agitated reactors, Chem. Eng. Sci. 52 (9) (1997) 1541–1551.
[44] N. Midoux, J.-C. Charpentier, Les réacteurs gaz–liquide à cuve agitée mécaniquement Partie 1: hydrodynamique, Entropie 88 (1979) 5–38.
[45] H. Yang, B.S. Fang, M. Reuss, $k_L a$ Correlation established on the basis of a neural network model, Can. J. Chem. Eng. 77 (1999) 838–843.
[46] F. García-Ochoa, E. Gómez Castro, Estimation of oxygen mass transfer coefficient in stirred tank reactors using artificial neural networks, Enzyme Microb. Technol. 28 (2001) 560–569.
[47] R. Lemoine, B. Fillion, A. Behkish, B.I. Morsi, A.E. Smith, Prediction of the gas–liquid volumetric mass transfer coefficient in surface-aeration and gas-inducing reactors using neural networks, Chem. Eng. Process. 42 (8–9) (2003) 621–643.
[48] R. Fuchs, D.D.Y. Ryu, A.E. Humphrey, Effect of surface aeration on the scale-up procedures for fermentation processes, Ind. Eng. Chem. Process Des. Dev. 10 (2) (1971) 190–196.
[49] G.Q. Martin, Gas-inducing reactors, Ind. Eng. Chem. Process Des. Dev. 11 (3) (1972) 397–404.
[50] B. Loiseau, Contribution à l'étude de l'hydrodynamique et du transfert de matière dans les réacteurs à cuve agitée mécaniquement, Ph.D. dissertation, INPL Nancy, France, 1976.
[51] R. Botton, D. Cosserat, J.C. Charpentier, Operating zone and scale up of mechanically stirred gas–liquid reactors, Chem. Eng. Sci. 35 (1980) 82–89.
[52] M. Greaves, M. Barigou, Estimation of gas hold-up and impeller power in a stirred vessel reactor, in Fluid Mixing III, Inst. Chem. Eng., Int. Chem. Eng. Symp. Series No. 108 (1988) 235–255.
[53] J.M. Smith, Simple performance correlations for agitated vessels, in: Proceedings of 7th Euro Congress on Mixing, Brugge, 1991, pp. 233–241.
[54] N. Koneripalli, in: M.S. Dissertation (Ed.), Mass Transfer Characteristics of Gases in Methanol and Ethanol Under Elevated Pressures and Temperatures in Agitated Reactors, University of Pittsburgh, Pittsburgh, PA, USA, 1992.
[55] T.I. Mizan, in: M.S. Dissertation (Ed.), Characterization of Mass Transfer of Gases in Olefinic Polymerization Solvents and Slurries in Agitated Reactors, University of Pittsburgh, Pittsburgh, PA, USA, 1992.
[56] C.D. Rielly, G.M. Evans, J.F. Davidson, K.J. Carpenter, Effect of vessel scaleup on the hydrodynamics of a self-aerating concave blade impeller, Chem. Eng. Sci. 47 (13–14) (1992) 3395–3402.
[57] V.B. Rewatkar, A.J. Deshpande, A.B. Pandit, J.B. Joshi, Gas hold-up behavior of mechanically agitated gas–liquid reactors using pitched blade downflow turbines, Can. J. Chem. Eng. 71 (1993) 226–237.
[58] C. Aldrich, J.S.J. van Deventer, Observations on the effect of medium density and viscosity on the rate of induced aeration in agitated vessels, Metall. Mater. Trans. B 25B (1994) 303–306.
[59] A.W. Nienow, G. Hunt, B.C. Buckland, A fluid dynamic study of the retrofitting of large agitated bioreactors: turbulent flow, Biotechnol. Bioeng. 44 (1994) 1177–1185.
[60] K. Saravanan, V.D. Mundale, J.B. Joshi, Gas inducing type mechanically agitated contactors, Ind. Eng. Chem. Res. 33 (1994) 2226–2241.
[61] C. Aldrich, J.S.J. van Deventer, Modelling of induced aeration in turbine aerators by use of radial basis function neural networks, Can. J. Chem. Eng. 73 (1995) 808–816.
[62] J. Li, Mass transfer and mathematical modeling for propylene polymerization process, Ph.D. Dissertation, University of Pittsburgh, Pittsburgh, PA, USA, 1995.
[63] K. Saravanan, J.B. Joshi, Gas-inducing-type mechanically agitated contactors: hydrodynamics characteristics of multiple impeller, Ind. Eng. Chem. Res. 34 (1995) 2499–2514.
[64] S.E. Forrester, C.D. Rielly, K.J. Carpenter, Gas-inducing impeller design and performance characteristics, Chem. Eng. Sci. 53 (1998) 603–615.
[65] G.P. Solomakha, T.A. Tarasova, Scale-up of mass transfer in mechanically agitated gas–liquid contactors, Theor. Found. Chem. Eng. 32 (5) (1998) 456–461.
[66] A. Mohammad, Gas–liquid mass transfer parameters in benzoic acid oxidation process, Ph.D. Dissertation, University of Pittsburgh, Pittsburgh, PA, USA, 1999.
[67] S.S. Patil, J.B. Joshi, Stability of gas-inducing type impeller, Can. J. Chem. Eng. 77 (1999) 793–803.
[68] P. Vrabel, R.G.J.M. van der Lans, K.Ch.A.M. Luyben, L. Boon, A.W. Nienow, Mixing in large-scale vessels stirred with multiple radial or radial and axial up-pumping impellers: modelling and measurements, Chem. Eng. Sci. 55 (2000) 5881–5896.
[69] M. Bouaifi, G. Hebrard, D. Bastoul, M. Roustan, A comparative study of gas hold-up, bubble size, interfacial area and mass transfer coefficients in stirred gas–liquid reactors and bubble columns, Chem. Eng. Process. 40 (2001) 97–111.
[70] S. Poncin, C. Nguyen, N. Midoux, J. Breysse, Hydrodynamics and volumetric gas–liquid mass transfer coefficient of a stirred vessel equipped with a gas-inducing impeller, Chem. Eng. Sci. 57 (2002) 3299–3306.
[71] A.A. Yawalkar, V.G. Pangarkar, A.A.C.M. Beenackers, Gas hold-up in stirred tank reactors, Can. J. Chem. Eng. 80 (2002) 158–166.
[72] S.S. Alves, C.I. Maia, J.M.T. Vasconcelos, Gas–liquid mass transfer coefficient in stirred tanks interpreted through bubble contamination kinetics, Chem. Eng. Process. 43 (2004) 823–830.
[73] R. Lemoine, A. Fillion, B.I. Morsi, Hydrodynamic and mass transfer parameters in agitated reactors Part I: critical mixing speed, induced gas flow rate, and wavy surface in SARs and GIRs, Int. J. Chem. React. Eng. 2 (2004) A29.
[74] V. Linek, M. Kordac, M. Fujasova, T. Moucha, Gas–liquid mass transfer coefficient in stirred tanks interpreted through models of idealized eddy structure of turbulence in the bubble vicinity, Chem. Eng. Process. 43 (2004) 1511–1517.
[75] Y. Heintz, R. Lemoine, L. Sehabiague, B.I. Morsi, Development and Testing of Fluorinated Liquids as CO_2 Solvents for High-Temperature and High-Pressure Applications, DOE Report 2005.
[76] J.-P. Soriano, in: M.S. Dissertation (Ed.), Mass Transfer Characteristics in an Agitated Slurry Reactor Operating under Fischer-Tropsch Conditions, University of Pittsburgh, Pittsburgh, PA, USA, 2005.
[77] A. Behkish, R. Lemoine, L. Sehabiague, R. Oukaci, B.I. Morsi, Prediction of the Gas holdup in industrial-scale bubble columns and slurry bubble column reactors using back-propagation neural networks, Int. J. Chem. React. Eng. (2005) in press.
[78] H.B.W. Patterson, Hydrogenation of Fats and Oils: Theory and Practice, American Oil Chemists Society Press, Champagne, 1994.
[79] A.E. Bailey, Bailey's Industrial Oil and Fat Products, vol. 2, fourth ed., John Wiley & Sons Inc., New York, 1979.
[80] K. Othmer, Encyclopedia of Chemical Technology, vol. 21, fourth ed., John Wiley and Sons Editions, New York, 1991.
[81] R.R. Allen, Hydrogenation of vegetable oils, J. Am. Oil Chem. Soc. 58 (1981) 166–169.
[82] I. Edvardsson, S. Irandoust, Reactors for hydrogenation of edible oils, J. Am. Oil Chem. Soc. 71 (3) (1994) 235–242.

[83] H. Topallar, Y. Bayrak, M. Iscan, Effect of hydrogenation on density and viscosity of sunflower seed oil, J. Am. Oil Chem. Soc. 72 (1995) 1519–1522.
[84] P.H. Calderbank, M.B. Moo-Young, The continuous phase heat and mass-transfer properties of dispersions, Chem. Eng. Sci. 16 (1961) 39–54.
[85] G. Marrucci, Rising velocity of a swarm of spherical bubbles, Ind. Chem. Eng. 4 (1965) 224.
[86] K. Saravanan, A.W. Patwardhan, V.D. Mundale, J.B. Joshi, Power consumption in gas inducing type mechanically agitated contactors, Ind. Eng. Chem. Res. 35 (1996) 1583–1602.